Available online at website: https://journal.bcrec.id/index.php/bcrec

Bulletin of Chemical Reaction Engineering & Catalysis, 19 (3) 2024, 480-499

Research Article

PbO_2/rGO Electrode as a Superior and Efficient Anode in Electrocatalytic Degradation of Safranine-O

Titin Aryani[1,2], Roto Roto[1], Mudasir Mudasir[1*]

[1]Department of Chemistry, Faculty of Mathematics and Natural Sciences, Universitas Gadjah Mada, Yogyakarta 55281, Indonesia
[2]Department of Medical Laboratory Technology, Faculty of Health Sciences, Universitas 'Aisyiyah Yogyakarta, Yogyakarta 55292, Indonesia

Received: 14th August 2024; Revised: 6th October 2024; Accepted: 7th October 2024
Available online: 9th October 2024; Published regularly: October 2024

Abstract

The electrocatalytic degradation method with PbO_2/rGO electrode (anode) was chosen to treat Safranine-O waste because it was cheap and environmentally friendly. This research aimed to study the electrocatalytic efficiency of PbO_2/rGO working electrode in Safranine-O removal. In this research, rGO and PbO_2/rGO electrodes were synthesized and applied to Safranine-O removal through electrochemical degradation. The characterization results of the morphology of rGO are in the form of a layered structure and have the atomic composition of C (82.87%) and O (17.13%). The characterization results of PbO_2/rGO are uniform particles with gaps/pores that appear relatively large. The rGO particles in the form of sheets (layers) seem to be distributed on the surface of PbO_2. PbO_2/rGO electrode has the atomic composition of C (87.24%), O (9.03), and Pb (3.73). The application of PbO_2/rGO anode to the electrochemical degradation of Safranine-O showed good performance. It was able to perform dye removal (DE%), as well as a decrease in BOD and COD values up to >95% within 10 minutes at a concentration of 20 ppm. Application on real waste also showed the ability of dye removal, COD, and BOD reduction up to >95%. Coating or modifying the PbO_2 anode with rGO can reduce the dissolution of Pb^{2+} ions in the solution during the electrochemical degradation. This study concluded that the PbO_2/rGO electrode has improved the efficiency in Safranine-O degradation.

Keywords: Waste; Electrochemical degradation; Dye; rGO; Lead Dioxide

How to Cite: T. Aryani, R. Roto, M. Mudasir (2024). PbO_2/rGO Electrode as a Superior and Efficient Anode in Electrocatalytic Degradation of Safranine-O. *Bulletin of Chemical Reaction Engineering & Catalysis*, 19 (3), 480-499 (doi: 10.9767/bcrec.20196)

Permalink/DOI: https://doi.org/10.9767/bcrec.20196

1. Introduction

Safranine-O (also known as Acid Red 2) is a dye used in industry and gram staining of bacteria in laboratories [1–12]. This dye has high stability, so it is difficult to degrade in aquatic ecosystems [11]. Safranine-O is used to distinguish between gram-positive and gram-negative microorganisms, resulting in effluents with a high concentration of Safranine-O dye [13–14]. These compounds are hazardous and carcinogenic and cause strong negative environmental impacts [3,15]. Proper treatment efficiency is required so that Safranine-O waste can be handled optimally.

Some methods of treating dye waste include coagulation/flotation methods [16,17], biological process [18], ozonization [19], electrochemical oxidation / electrodegradation [20,21], and adsorption [22]. The adsorption method is still considered an incomplete treatment method because the compounds adsorbed by the adsorbent material will remain in the system and can one day be released back into the environment, so the potential for pollution still occur. Waste processing methods that convert dye waste into safe and environmentally friendly end products

* Corresponding Author.
Email: mudasir@ugm.ac.id (M. Mudasir)

include electrodegradation (electrochemical oxidation) [20,21,23]. Electrodegradation can be carried out under mild operating conditions, at ambient temperature and pressure, and has the potential to produce CO_2 and H_2O as end products [24]. Electrochemical oxidation is also a cost-effective method, which is characterized by strong oxidative species with high performance [20]. The electrochemical oxidation process does not require the addition of hazardous chemicals and produces virtually no secondary pollutants at the end of the treatment [25,26].

Some researchers have used degradation techniques through electrochemical oxidation (electrodegradation) to reduce the concentration of dye waste [25,26]. The results show that the electrochemical oxidation / electrodegradation efficiency is highly dependent on the properties of the electrode materials and operational conditions [27]. Some of the electrodes used for dye oxidation are expensive, such as boron-doped diamond (BDD), IrO_2, RuO, and Pt [23,28]. Some scientists focus more on the PbO_2 electrode as an anode because of its low price, high electronic conductivity, relatively stable in corrosive media, and relatively high oxygen evolution reaction potential [29-31]. PbO_2 can produce hydroxyl radicals, which are adsorbed on the PbO_2 anode in positive polarization in the water oxidation region: $PbO_2 + H_2O \rightleftharpoons PbO_2(OH^{\cdot}) + H^+ + e^-$

Hydroxyl radicals ($OH^{\cdot}$) can degrade almost all organic pollutants due to their high oxidation ability and non-selectiveness to organic micropollutants [32]. The large surface area of the porous PbO_2 electrode facilitates the oxidation reaction, thereby increasing the efficiency of the electrodegradation of dye waste. The electrodegradation reaction using a PbO_2 electrode with NaCl electrolyte is an oxidation reaction involving the oxidizer $^{\cdot}OH$ and Cl_2 and ClO^- produced from the oxidation process of chloride ions in solution [15].

PbO_2 electrodes (anodes) have been reported to be able to dye degradation [21,33-35]. However, at currents that tend to be high, the Pb metal in the PbO_2 electrode can dissolve as Pb^{2+}, so this is a weakness of this electrode because it can cause surface changes and reduce electrode performance in the electrodegradation, as well as produce new pollutants (Pb^{2+}) and cause new problems [35-39]. In addition, the electrodegradation capability of the PbO_2 electrode still shows relatively low efficiency because it takes a relatively long time to completely degrade the dye [34,35,40-42]. This means it is still necessary to improve the performance of the PbO_2 electrode in electrodegradation by increasing the conductivity and stability of the electrode. One method that can be applied to overcome this problem is to modify the PbO_2 electrode with an appropriate modifier [33].

Researchers have proven that graphene is a good modifier for coating PbO_2 anodes [21,43]. Graphene with oxygen functional groups into graphene oxide (GO) and reduced graphene oxide (rGO) shows high electrocatalytic performance for dye degradation [21,43,44]. GO contains more functional groups than rGO. The main functional groups in GO and rGO are epoxide and hydroxyl on the basal plane and carbonyl, quinone, carboxylic acid, phenol, and lactone groups on the edges. More functional groups in GO cause chemical reactivity that damages the properties of graphene, thereby reducing conductivity, causing structural defects, and reducing thermal and mechanical stability [45]. Therefore, choosing graphene materials with fewer functional groups, such as rGO, is essential.

Currently, although rGO or other graphene is known to have good conductivity and electrocatalytic ability, in general, researchers use rGO or graphene more as a modifier and not as an anode directly or as a main electrode (substrate) [46–49]. Its effectiveness and efficiency are still considered less when compared to rGO as a modifier because it requires more rGO material to form the main electrode (substrate), while rGO or graphene materials are relatively expensive [49]. The high price of rGO is caused by the synthesis method, which is relatively difficult and has few results [50]. In addition, using rGO as a main electrode or substrate electrode (not a modifier) requires difficult additional treatment because initially, in powder form, it changes into a plate or rod. Using rGO as a modifier, especially on electrodes with a low price, such as PbO_2, increases the conductivity and the oxidizer in the form of hydroxyl radicals of the rGO functional group. In the end, the effectiveness and efficiency of electrode use becomes higher. In addition, rGO can coat PbO_2 and reduce or eliminate Pb dissolution so that the weaknesses of the PbO_2 electrode can be overcome.

The method often used for rGO synthesis is the GO reduction method, which uses either a chemical reductant (e.g. hydrazine and sodium bicarbonate) or natural materials (plant extracts) [51-53]. The Hummer method synthesizes GO as a rGO precursor using hazardous materials such as sulfuric acid and potassium permanganate [53–55]. Another alternative in rGO synthesis is the reduction method using a carbon source [56–60]. Previous research has not used the hydrothermal method to synthesize rGO from the charcoal activated material. In this study, rGO is synthesized using a more environmentally friendly hydrothermal method, distilled water as a solvent, with relatively fast hydrothermal time (12 hours) and without hazardous chemicals. By hydrothermal reduction treatment, charcoal activated molecules with almost no aliphatic

chains are expected to maintain or increase the sp2 carbon content after changing into rGO.

The modification of the PbO_2 anode with an rGO modifier into PbO_2/rGO in this study was done using the electrophoretic deposition (EPD) method. Several studies have explored the EPD method for graphene coating on metal electrode plates, for example, coating SS electrodes with graphene functionalized hydroxyl (G-OH) to form SS/G-OH and coating SS electrodes with rGO to form SS/rGO [61,62]. However, no study has explored the coating of PbO_2 electrodes with rGO material, especially rGO synthesized using the hydrothermal method with charcoal activated precursors. The rGO synthesis method, the EPD method for PbO_2 coating to form PbO_2/rGO, and its application to the electrodegradation of Safranine-O dye are novelties in this study. To understand this, this study aims to determine the characteristics of rGO and PbO_2/rGO synthesized and their applications to the electrodegradation of Safranine-O dye. The characterization of rGO and PbO_2/rGO was studied using UV-Vis spectrophotometers, FTIR spectrophotometers, X-ray Diffraction (XRD), Raman spectroscopy, Scanning Electron Microscope-Energy Dispersive X-ray Fluorescence (SEM-EDX), and Transmission Electron Microscope (TEM). To determine the electrocatalytic ability of rGO and modified electrodes (PbO_2/rGO) were confirmed using cyclic voltammetry (Potensiostat) before being used to remove Safranine-O through electrodegradation using NaCl electrolyte. NaCl is a supporting electrolyte that can oxidize Cl^- to Cl_2 [21]. The Cl_2 improves the electrocatalytic performance of the PbO_2/rGO electrode. The progress of the electrodegradation process was monitored by Uv-Vis Spectrophotometry. Chemical Oxygen Demand (COD) was analyzed using the Closed Reflux Colorimetry method, and Biological Oxygen Demand (BOD) of waste was analyzed using a DO meter. The level of Pb dissolved in the degradation solution was analyzed using Atomic Absorption Spectrophotometry (AAS).

2. Methods

2.1 Chemicals

This study used sulfuric acid p.a (H_2SO_4>95-97%), sodium chloride p.a (NaCl >99%), acetone p.a (C_3H_6O>99%), hydrochloric acid p.a (HCl>37%), lithium hydroxide p.a (LiOH ≥ 98%), sodium hydroxide p.a (NaOH ≥ 97%) from Merck Germany, and Safranine-O p.a purchased from Sigma Aldrich, U.S.A ($C_{20}H_{19}ClN_4$ >80%). Stainless steel 316L plates from the local Indonesian product (TB. Bintang Logam). Lead plates (Pb≥99%) are obtained from the local Indonesian products (TB. Timbah Bangka Indonesia). Commercial charcoal activated obtained from Loba Chemie PVT.LTD, India. All chemical reagents used in this study were analytical grade and used without further purification.

2.2 Instrumentation

In this study, the absorption peak characteristic of rGO in the UV region, which is the π to π* transition of C=C bonds of the hexagonal structure of rGO, was analyzed using 50 mg/100mL rGO suspension at a wave number of 200–800 nm with a UV-Vis spectrophotometer (Thermo Scientific Genesys 180). All functional groups of rGO and PbO_2/rGO were characterized using Fourier Transform Infra-Red Spectrophotometry (FTIR, Thermo Scientific Nicolet iS10) using the KBr pellet technique at a wavelength of 4000–400 cm^{-1}). The characteristics of the crystal structure of rGO and PbO_2/rGO and the presence of diffraction lines and characteristic diffraction peaks were analyzed using X-ray diffraction (XRD, Simadzu model XRD-6000 with a Cu X-ray tube, Kα = 1.5406 Å, and scanning at 2θ = 5–60˚).The characteristics of the carbon material (charcoal) and the level of carbon defects in rGO were analyzed using a Raman spectrometer (Horiba Scientific Raman spectrometer equipped with LabSpec 6 software). The surface morphological characteristics and elemental composition of rGO and PbO_2/rGO were analyzed using a Scanning Electron Microscopy-Dispersive X-ray spectrometer (SEM-EDX, JEOL JSM-6510). The character of the particle shape and layer structure of rGO material were analyzed using a transmission electron microscope (TEM, JEOL JEM-1400).

2.3 Synthesis of rGO

In this research, rGO synthesis was carried out using a hydrothermal autoclave reactor with a PTFE chamber with a capacity of 100 mL purchased from China. Particles were sedimented using a centrifuge (Hettich EBA 200). Digital ultrasonics (GT Sonic 40 KHz, 100W) was used to reduce the agglomeration of rGO particles to obtain a better size distribution. rGO synthesis was done by making a charcoal activated solution by weighing 0.1 grams of charcoal activated and then dissolving it in 100 mL of aquabides. The charcoal activated solution was put into an autoclave for a hydrothermal process for 12 hours at 190 ^{0}C. After the hydrothermal method, ultrasonication was carried out for 1 hour, and the solution was centrifuged. The ultrasonicated product was washed, filtered, and then dried in an oven at 80 °C for 2 hours for characterization.

2.4 Synthesis of PbO_2 Electrode

The synthesis of the PbO_2 anode was carried out by sanding a lead (Pb) electrode plate with dimensions of 5.0 cm × 2.0 cm and thickness 2 mm, cleaned using detergent, and then ultrasonicated (with ultrasonic cleaner, GT Sonic 40 kHz, 100 W) sequentially using 30% NaOH for 30 min, 3.75% HCl and acetone for 10 min. Next, electrolysis of Pb metal was performed. In the electrolysis process, Pb acts as an anode and stainless steel as a cathode. Industrial DC power supply (Sanfix SP-305E) was used as a source of electric current in PbO_2 electrode synthesis. Electrolysis was carried out using 100 mL H_2SO_4 10% electrolyte and a current strength of 1 A for 30 minutes.

2.5 Synthesis of PbO_2/rGO Electrode

The PbO_2/rGO anode was synthesized by depositing rGO on the surface of the PbO_2 electrode. Industrial DC power supply (Sanfix SP-305E) was used as a source of electric current. Electrophoretic deposition (EPD) of rGO was carried out by immersing the PbO_2 as the anode and the stainless steel plate as the cathode in a 2 g/L rGO dispersion. The process was supplied with a current density of 10 mA/cm^2 for 10 minutes. Cyclic voltammetry (CV) of the PbO_2/rGO working electrode was recorded using Corrtest Potentiostat. Platinum (Pt) electrode as cathode and Ag/AgCl electrode as reference electrode. The CV was measured in the supporting electrolyte of 0.1 M NaCl.

2.5 Electrocatalytic Performance Test of rGO Material and PbO_2/rGO Electrode

Potentiostat (Corrtest Potentiostat) was used to analyze the electrocatalytic ability of rGO compared to bare electrode (Glassy carbon electrode, GCE) and to compare the electrocatalytic ability of both PbO_2 and PbO_2/rGO electrodes by observing the change in peak current as a function of potential using cyclic voltammetry (CV) technique. Electrocatalytic measurements of rGO material were carried out with a glassy carbon working electrode (GCE) modified by rGO. This measurement uses an Ag/AgCl electrode as a standard electrode and a Pt electrode as a cathode. The electrolyte used in this electrocatalytic measurement is 0.10 M NaCl. The scan rate used was 50mV/s in the potential range of -0.6 to 0.8 V. Electrocatalytic measurement of PbO_2/rGO anode was conducted with PbO_2/rGO electrode as working electrode, and Ag/AgCl electrode as a standard electrode, and Pt electrode as a cathode. The electrolyte used in this electrocatalytic measurement was 0.10 M NaCl. The scan rate was 50 mV/s in the potential range of -1.2 to 0.8 V.

2.6 Electrocatalytic Degradation of Safranine-O

Electrocatalytic degradation of Safranine-O was carried out using a batch-type electrolysis cell and a DC power supply. Industrial DC power supply (Sanfix SP-305E) was used as a source of electric current. PbO_2/rGO acted as the working electrode (anode) with a stainless-steel cathode. The electrolyte was 100 mL NaCl 0,1 M. Dye waste was 100 mL Safranine-O 20 ppm. The current density was 50 mA/cm^2. The initial pH solution was 7.0. Safranine-O removal in simulated and real waste was measured by UV-Vis spectrophotometry. Decreased absorbance (DA (%)) and Degradation efficiency (DE (%)) were calculated by using the following Equation (1) and Equation (2) [63]:

$$DA(\%) = \frac{A_0 - A_t}{A_0} \times 100\% \quad (1)$$

A_o and A_t are the initial absorbance and absorbance at the sampling time of t, respectively.

$$DE(\%) = \frac{C_0 - C_t}{C_0} \times 100\% \quad (2)$$

C_o and C_t are the initial concentrations and concentrations at the sampling time of t, respectively.

The lead levels in the post-electrodegradation solution were analyzed using an atomic absorption spectrophotometer (AAS, Shimadzu 6650 F). Chemical oxygen demand (COD) was analyzed by Standard Method as described in the 20th Edition - Examination of Water & Waste Water, Methods 5220-D-Closed Reflux Colorimetric Methods by spectrophotometer at a wavelength of 620 nm [64]. Biological oxygen demand (COD) was analyzed using a DO meter by standard methods for the examination of water and wastewater 21th edition L.S Clesceri, A.E Greenberg, A.D Eaton, APHA, AWWA, and WPCF, Washington DC (2005) [65.

The kinetic study of the data was evaluated by applying pseudo-first-order and pseudo-second-order kinetics equations (Equation (3)) [66]:

$$ln\left({C_t}/{C_0}\right) = -Kt \quad (3)$$

$$\frac{1}{C_t} = \frac{1}{C_0} + Kt \quad (4)$$

3. Results and Discussion

3.1 Synthesis of rGO

The synthesis of rGO in this study used the hydrothermal method. The synthesis mechanism of rGO proposed in this study is illustrated in Figure 1. In the hydrothermal process, the first mechanism proposed for the formation of rGO is that during the heating process, charcoal activated undergoes a wet pyrolysis process to

form a series of small molecular hydrolysis products such as aromatic compounds, polysaccharides, aldehydes, ketones, and furan derivatives. Secondly, under the hydrothermal condition of 190 ^{0}C for 12 h, the pyrolysis products self-assembly into nanosheet structures through intermolecular hydrogen bonding at the beginning of the reaction, and then a hexagonal graphite matrix with multiple functional groups is formed due to intermolecular dehydration between carboxyl groups and hydroxyl groups. Furthermore, the graphite nanosheet undergoes exfoliation and reduction under hydrothermal conditions to form rGO. This research is in line with previous research [67–69]. Ultrasonication in this study reduces the agglomeration of rGO particles to obtain a better size distribution, while centrifugation separates the precipitated particles [70].

Previous researchers obtained similar results, stating that hydrothermal works by decomposing biomass through a series of liquid-phase reactions (e.g., dehydration, Diels-Alder, fragmentation, retro-aldol, and condensation). The study's XPS, FTIR, and NMR results showed that hydrothermal caused condensation of aromatic structures, as evidenced by increased carbon in XPS data and aromatic region in NMR (~130 ppm). Some of the carboxylic acids were lost on the surface of the carbon structure and replaced by alcohols and ethers [68,69].

3.2 Characterizations of rGO

Figure 2 shows the Uv-Vis Spectra of rGO. A single peak was observed at 266 nm. This peak is the result of π to π* excitation of the C=C bond in the hexagonal structure of rGO [71–73]. Figure 3 shows the characteristic FTIR spectra of rGO produced through the hydrothermal process [74,75]. The peak at 3425 cm^{-1} is an O–H stretching vibration. The spectra show a small peak at 2915 cm^{-1}, which is a Csp-H stretching vibration. The peak at 1565 cm^{-1} is a C=C stretching vibration. C–O is seen at 1136 cm^{-1} peak. All FTIR peaks agree with previous research [76–78]. The hydrothermal process causes a reduction in oxygen-containing

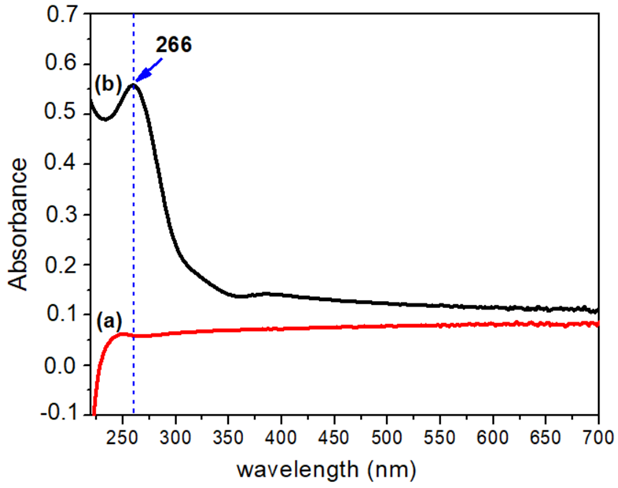

Figure 2. Uv-Vis spectra of (a) charcoal activated, (b) rGO

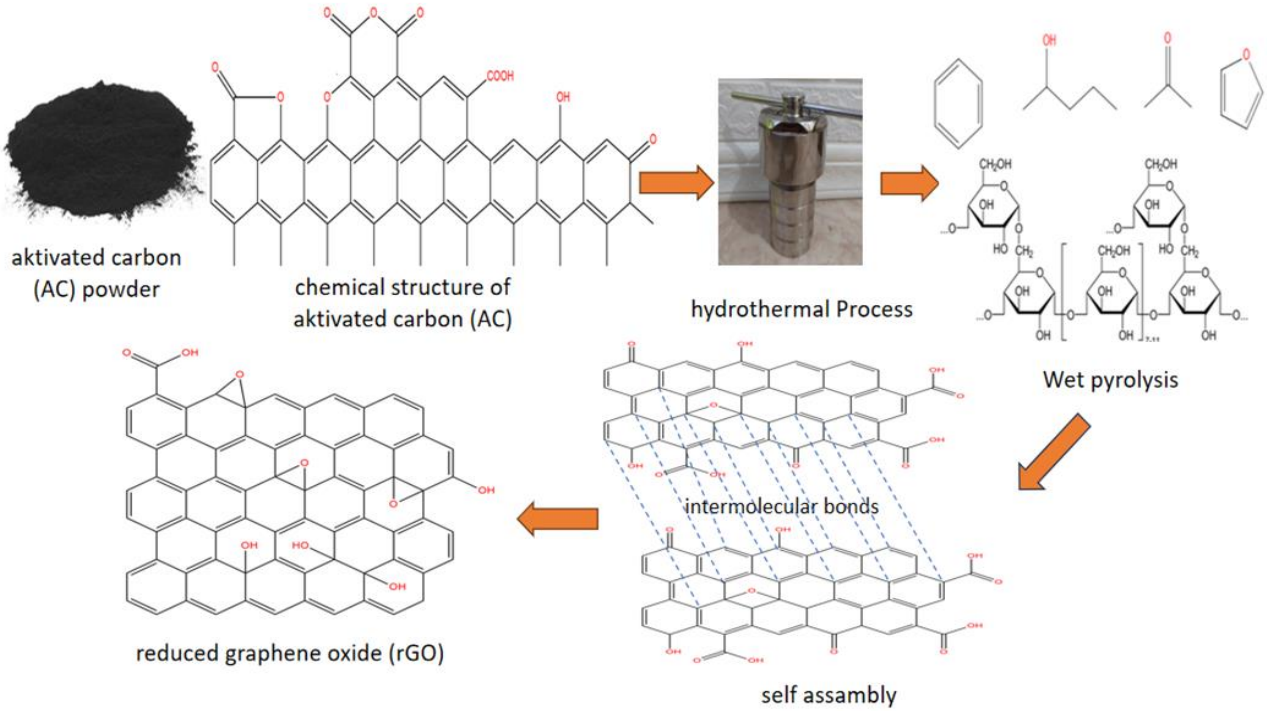

Figure 1. Proposed synthesis mechanism of rGO

functional groups. This is characterized by a decrease in the peaks related to the –OH groups at 3425 cm^{-1} and C–O groups at 1136 cm^{-1}. The XRD pattern of rGO in Figure 3 shows a broadening of the diffraction peak at 24.59⁰. This corresponds to the (002) plane of the graphene crystal. Figure 4 shows that the XRD pattern obtained corresponds to previous studies [72,78,79]. In this study, the shift in the peak broadening of rGO occurred because, in the reduction process, oxygen groups were removed and bound to charcoal activated so that it could change the distance between layers and cause a peak shift [80].

In Figure 5, the Raman spectra results show two peaks at Raman shifts of 1335.77 and 1595.67 cm^{-1}. The appearance of the peak at 1335.77 cm^{-1} indicates the D band (defect), which is produced from out-of-plane vibrations that may be caused by wrinkled structures and defects. The G band (graphite) appears at 1595.67 cm^{-1} due to the in-plane vibrations of carbon atoms with sp2 hybridization [81]. The degree of disorder is determined by the ratio of the D/G peak intensity (I_D/I_G). Charcoal activated has an I_D value of 151 and an I_G of 150 counts, while rGO has an I_D value of 224 and an I_G value of 201 counts. The I_D/I_G ratios of charcoal activated and rGO are 1.006 and 1.114. The broadening of the D and G bands in rGO occurs due to higher interference with an increase in the relative intensity of the D band compared to the G band [80]. The D band's higher intensity in rGO than charcoal activated is due to removing oxygen functional groups from activated carbon after reduction. The broad and short peak at ~2700 cm^{-1} is attributed to the splitting of 2D peaks, implying increased vibrational modes [81].

When charcoal activated is reduced to rGO, the I_D/I_G value should decrease due to eliminating some oxygen-containing functional groups during the reduction process. This results in a decrease in defects caused by oxygen or oxygen-containing functional groups. In contrast, the results of this study show that the I_D/I_G value has increased. Therefore, the I_D/I_G ratio value may not only be based on eliminating some oxygen functional groups, but other effects may also occur. The functionalization of sp3 groups and defects in the carbon structure in rGO causes a D peak. The removal of functional groups on the surface of charcoal activated by the reduction process results in vacancies and rearrangement of the carbon structure so that the originally sp3 carbon atoms do not become sp2 in rGO and the carbon structure becomes five-ring (pentagonal) or seven-ring (heptagonal) [77].

Figures 6a and 6b show the SEM-EDX results of the charcoal activated and the synthesized rGO. SEM results show that charcoal activated has a morphology in the form of a structure containing pores/gaps, small particles that are almost uniform without any layers formed, while rGO has a morphology in the form of a layered structure in the form of overlapping sheets resulting in gaps or

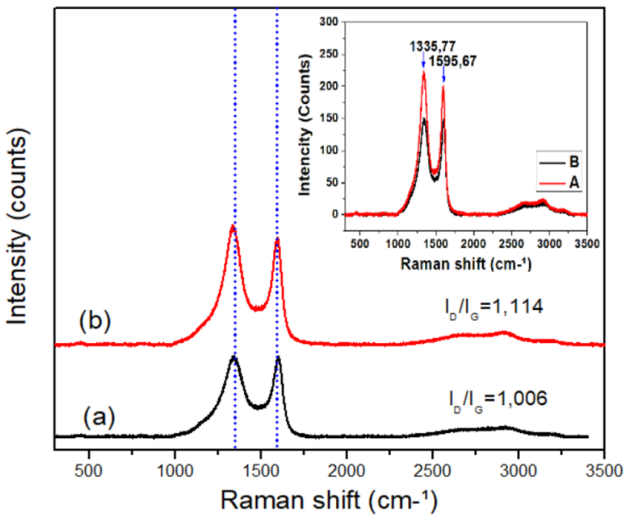

Figure 5. Raman spectra of (a) charcoal activated, (b) rGO

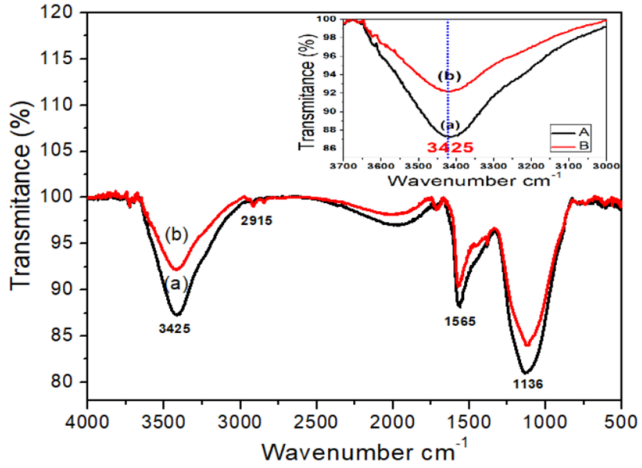

Figure 3. FTIR spectra of (a) charcoal activated, (b) rGO

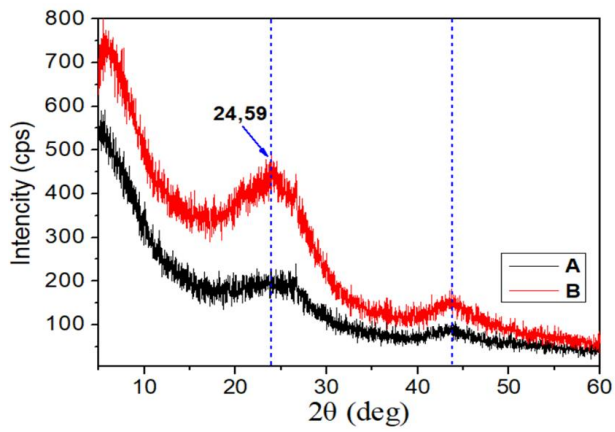

Figure 4. XRD patterns of (a) charcoal activated, (b) rGO

distances between layers, and particle agglomeration occurs. The agglomeration can be caused by removing oxygen-containing groups through the reduction process, thereby reducing the electrostatic repulsion between the graphene layers, which can cause the particles to approach each other and form agglomerations [82]. The EDX results show that charcoal activated has an atomic composition of C (78.60%) and O (41.40%), while rGO has a composition of C (82.87%) and O (17.13%). These data indicate that charcoal activated experiences a decrease in the number of oxygen atoms and an increase in the number of carbon after being reduced to produce rGO [83].

Figures 7a and 7b show TEM results of the charcoal activated and the synthesized rGO. TEM results show that the morphology of rGO has an irregular shape and does not have a layered structure, while rGO has a typical sheet shape and a layered structure with a regular shape, especially rGO produced in multilayer form. The irregular shape is a characteristic of charcoal activated, while rGO has a typical sheet shape [51,84]. This layered structure of rGO indicates that the rGO formed is a multilayer rGO. SEM results support these TEM results, which show a layered structure in rGO.

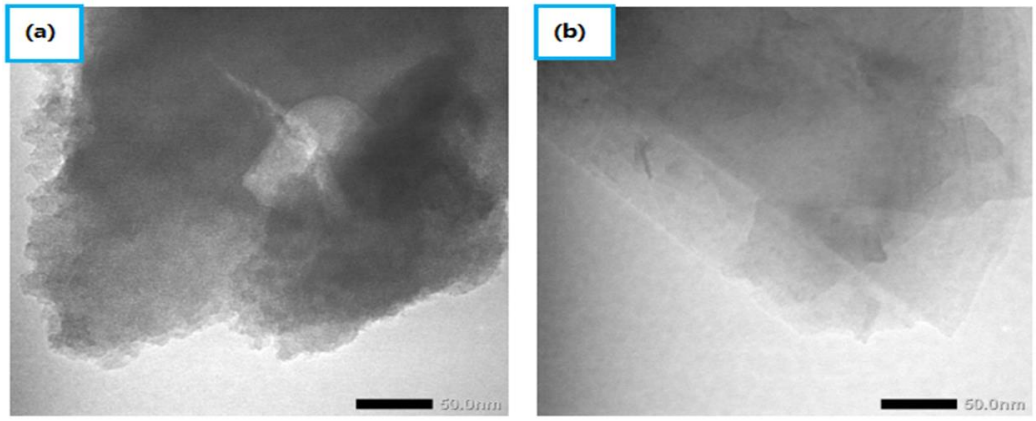

Figure 7. TEM results on materials a) charcoal activated, b) rGO

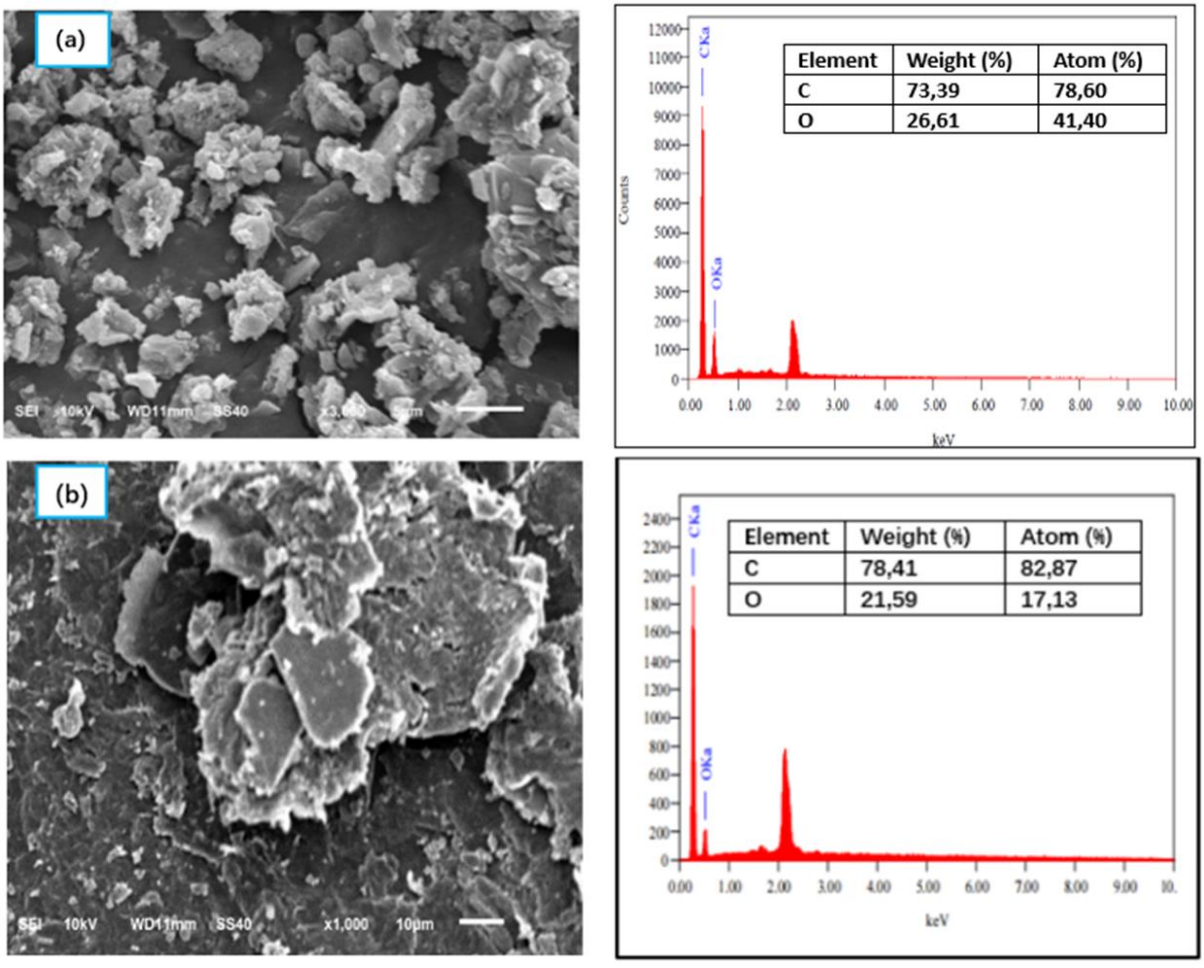

Figure 6. SEM-EDX results on materials, a) charcoal activated, b) rGO

3.3. Synthesis of PbO_2/rGO Electrode

The synthesis of the PbO_2/rGO electrode was carried out by synthesizing the PbO_2 anode first. Synthesis of PbO_2 anode is done by an anodic electrodeposition method using a Pb anode, stainless steel cathode, and H_2SO_4 electrolyte. The reaction mechanism that occurs is shown in Equations (5–6) [85,86].

Reaction at the anode (Oxidation):

$$Pb \rightarrow Pb^{2+} + 2e^- \quad (5)$$

$$Pb^{2+} + 2H_2O \rightarrow PbO_2 + 4H^+ + 2e^- \quad (6)$$

PbO_2 anodes are formed due to the oxidation of Pb to Pb^{2+}, and then Pb^{2+} produces Pb^{4+}, which then forms a PbO_2 anode. The electrocatalytic properties of the PbO_2 anode are caused by the successful electrodeposition of O_2, which will then produce hydroxyl radicals (see Equation (7)). Hydroxyl radicals ($^{\cdot}OH$) have strong oxidizing properties [87]. When an electrical voltage is applied, the PbO_2 anode allows the direct oxidation of Safranin-O dissolved in the electrolyte solution to produce simpler products, such as carbon dioxide, water, and other simple compounds (intermediate compounds) [87].

$$PbO_2 + H_2O \rightarrow PbO_2(^{\cdot}OH) + H^+ + e^- \quad (7)$$

The PbO_2 anode is then used as an anode for electrophoretic deposition of rGO to form PbO_2/rGO. The reaction mechanism that occurs is shown in Equation (8) [68].

$$PbO_2 + rGO \rightarrow PbO_2/rGO \quad (8)$$

Figure 8 shows that initially, the PbO_2 electrode was dark brown, then after being coated with rGO, the electrode surface turned black due to the attachment of rGO. The mechanism of rGO attachment to the PbO_2 electrode is that when rGO is dissolved in water, the functional groups of rGO undergo dissociation in water and produce a negative charge. With voltage, the negative charge of rGO moves towards the positively charged electrode (anode) and then sticks tightly to the anode surface. This opinion is supported by previous studies that stated something similar [61,88,89].

Table 1 shows the data of successful electrode synthesis using various substrates and graphene using the EPD method [61,62,68,88,90-94]. The results showed that multiple studies used different voltages, current densities, times, and types of graphene (rGO, GO, graphene, sulfonated rGO, and G-OH). In this study, the voltage/current density applied was not too high (10 mA/cm^2) and not too long (10 minutes), so it was possible that rGO would not undergo oxidation to become GO during EPD. Oxidation of rGO to GO requires high voltage/current density and a relatively long time to increase the possibility of rGO oxidation to GO. Several studies in Table 1 do not explain the oxidation of rGO to GO when EPD is applied, so further studies are still needed to confirm this.

In the EPD of graphene (rGO) on metal (substrate electrode, for example, PbO_2), it is generally impossible to say that this process is entirely free from redox reactions. However, under some conditions, especially when only graphene (rGO) particles are transferred using low voltages, redox reactions may insignificantly occur [61]. This is because the current flow tends to be smaller at low voltages, so the possibility of redox reactions is lower. Under these conditions, transferring graphene (rGO) particles to the metal surface is more dominant than the redox reactions. Redox reactions may still occur, but the effects may be minimal.

The thickness and quality of this layer are controlled by adjusting the deposition time and electric field strength [88,95]. The best deposition time should be selected considering that too long a time can cause excessive consumption of material resources and increase the coating

Table 1. Overview of the substrate/graphene prepared by EPD

EPD Substrat	Graphene (modifier type)	Voltage/current density	Time (minutes)	Ref.
SS	rGO	6-8 Volt	10	[61]
SS foil	Graphene	30 Volt	2	[90]
TiO_2 nanotube	rGO	4 Volt	30	[91]
Carbon fiber cloth	Sulphonated-RGO	20 V	30	[92]
Copper	GO	5 Volt	10	[93]
Carbon fibers	rGO	15 Volt	-	[94]
SS	GO	10 Volt	8	[88]
SS	G-OH	30 V	3	[62]
Pb/PbO_2	rGO	10 mA/cm^2	10	[68]
PbO_2	rGO	10 mA/cm^2	10	This work

thickness. Too thick a coating can affect the conductivity properties and activity of the electrode. Too long an EPD time can cause aggregation of rGO particles, which can reduce the quality of the coating and disrupt its even distribution. Conversely, a time that is too short may not be enough to obtain an optimal coating [88].

The CV voltammogram results in Figure 9 show that time affects the EPD or attachment of rGO on the PbO_2 electrode. At an EPD time of 0 minutes, the PbO_2 electrode shows a peak oxidation current of 0.437 V and 0.007 A. Then, the increase in peak oxidation current continues to occur until it reaches the optimum point. The optimum point occurs after reaching an EPD time of 10 minutes with a peak oxidation current of 0.371 V and 0.014 A. The increase in the oxidation current peak indicates that there has been an increase in the number of rGO layers deposited on the PbO_2 electrode, thereby increasing the electrochemical capacity, which is caused by increasing the active surface area or the number of active sites available for the reaction [89]. The peak oxidation current decreased after passing the optimum point (at 12.5 minutes). The decrease in the peak oxidation current indicates that the rGO layer begins to accumulate or aggregate. This can cause pore closure or reduction in effective surface area, thereby reducing the availability of active sites for reaction and decreasing electrochemical capacity. These results are in accordance with previous studies [68,89].

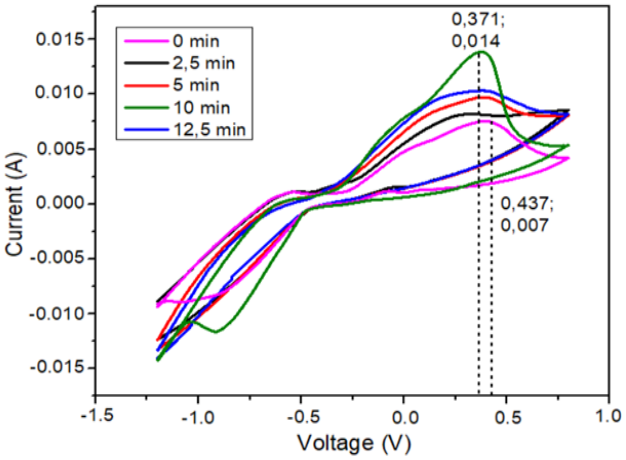

Figure 9. Cyclic voltammogram of PbO_2/rGO anode in 0.1 M NaCl based on deposition time variation

3.4. Characterizations of PbO_2/rGO Electrode

Characterization of PbO_2/rGO electrode was carried out by analyzing it using XRD and SEM-EDX. Figure 10 shows that the XRD pattern confirmed the presence of PbO_2 and all diffraction peaks could be indexed into the standard spectrum of β-PbO_2 according to JCPDF (PDF File No. 752420). The result of XRD in Figure 10 shows that the crystal structure of PbO_2 in an acid solution is pure β-PbO_2 [87]. Only a few impurity peaks are visible. Sharp peak intensity validates high crystallinity [96]. The electrophoretic deposition of rGO on the PbO_2 anode leaves a characteristic peak for rGO and PbO_2 in the PbO_2/rGO material, where the XRD pattern still shows a typical peak belonging to rGO at 2θ around 25^0.

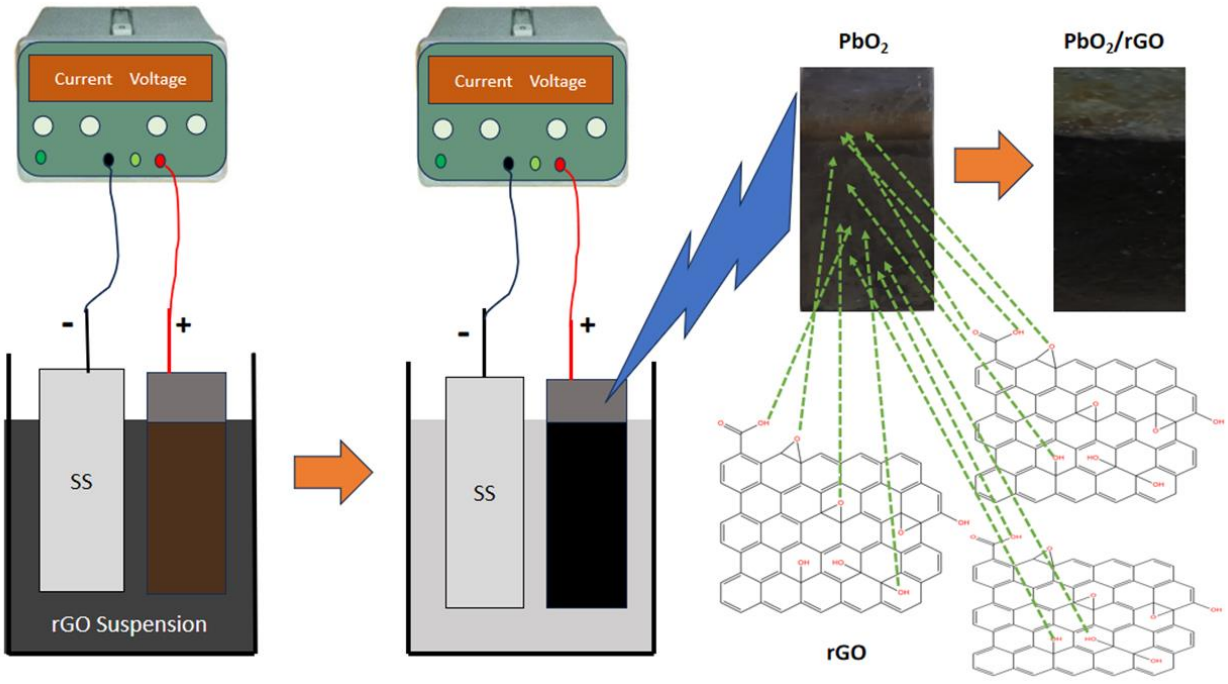

Figure 8. Synthesis mechanism of PbO_2/rGO electrode

Figures 11a and 11b show the SEM-EDX results of PbO_2 and PbO_2/rGO. The morphology of PbO_2 is in the form of tightly packed particles, causing the gaps/pores to appear smaller, while PbO_2/rGO has uniform particles with gaps/pores that appear relatively larger. The rGO particles in the form of sheets (layers) seem to be distributed on the surface of PbO_2. This proves that rGO has successfully coated the surface of PbO_2. This porous morphology is important for transferring pollutants in the degradation process. The SEM-EDX results show that in the PbO_2 electrode, no carbon element was detected, while the PbO_2/rGO material revealed the presence of carbon elements. The carbon element of the PbO_2/rGO electrode has an atomic percentage of 87.24%. The atomic composition of the PbO_2/rGO material is C (87.24%), Pb (29.33%), and O (9.03%). This result follows previous research [68].

3.5 Electrocatalytic Performance Test of rGO Material

Cyclic voltammograms of the rGO material were measured to determine its electrocatalytic ability when used as an electrode modifier. Figure 12 shows that the Glassy Carbon (GCE) electrode without rGO modification showed an oxidation current peak centered at a voltage of 0.58 V and a current of 406.37 mA, while the rGO-modified GCE electrode showed an oxidation current peak centered at a voltage of 0.36 V and a current of 492.307 mA. This proves that modifying the electrode surface with electroactive species increases the electron transfer rate and produces a larger current than the electrode without modification. This data further reinforces that

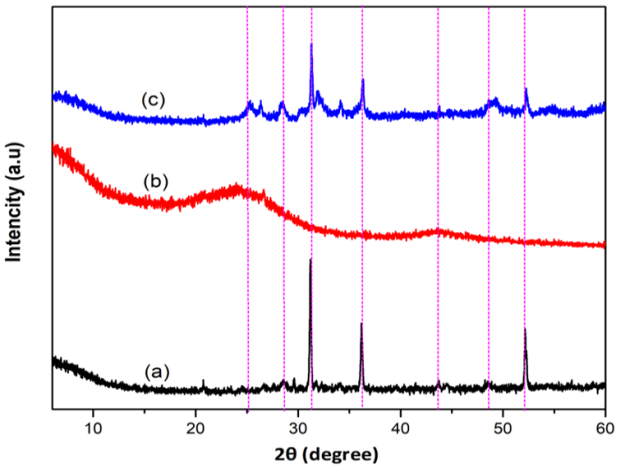

Figure 10. Material diffractograms, a) PbO_2, b) rGO, c) PbO_2/rGO

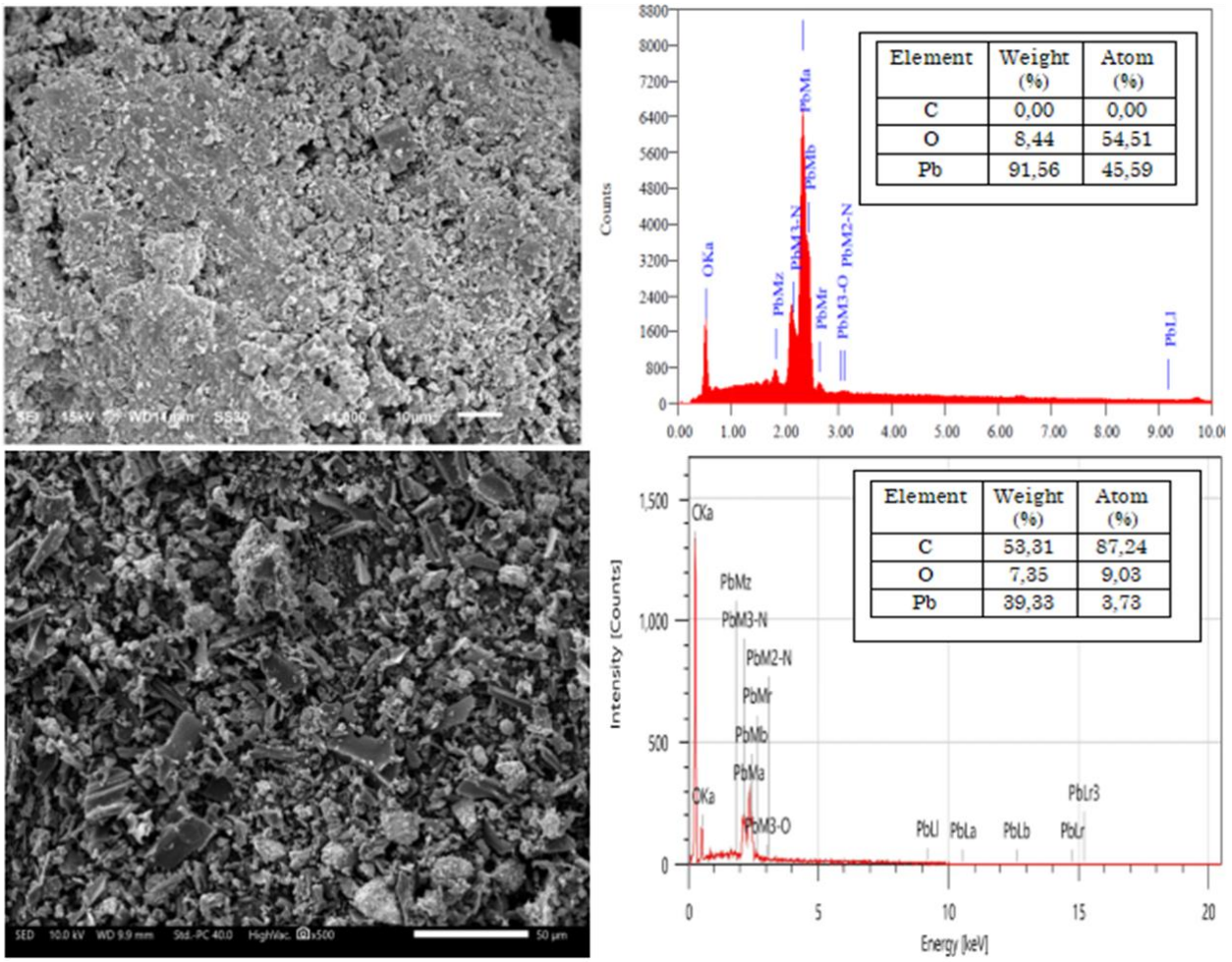

Figure 11. SEM-EDX results on the material, a) PbO_2, b) PbO_2/rGO

rGO exhibits good electrocatalytic capabilities when used as an electrode modifier.

The PbO_2/rGO electrode (anode) was measured to understand the redox process of the modified electrode. Figure 13 shows the resulting CV voltammogram. rGO was deposited on the PbO_2 anode by electrophoretic deposition reaction. The PbO_2 anode without rGO modification (EPD time 0 minutes) shows an oxidation current peak centred on a voltage of 0.437 V and a current of 0.007 A. The PbO_2/rGO modified electrode (EPD time 10 minutes) shows an oxidation current peak centred on a voltage of 0.371 V and a current of 0.014 A. When compared to the PbO_2 electrode, the PbO_2/rGO anode shows a decrease in voltage accompanied by an increase in the oxidation current peak, indicating that the redox process on the PbO_2/rGO anode can occur more easily than the PbO_2 electrode and rGO on the PbO_2/rGO electrode can act as an electrocatalyst in the NaCl electrolysis reaction. Oxidation of Cl^- to Cl_2 and reduction of Cl_2 to Cl^- occur during oxidation and reduction scanning. This process occurs more easily on PbO_2/rGO electrodes than on PbO_2 [68].

3.6 Electrocatalytic Degradation of Safranine-O

In this study, the dye we used was Safranine-O. Safranine-O has an absorbance peak in the ultraviolet light region of 285 nm and visible light of 520 nm. Adding NaCl to the electrolyte solution in the electrocatalysis degradation process can increase the conductivity of the solution. This can increase the efficiency of the electrolysis process because higher conductivity facilitates electron transfer and produces more hydroxyl radicals. In addition, NaCl is a source of chloride ions that produce free chlorine and hypochlorite ions. In this study, the concentration of NaCl used was 0.1 M. Excess electrolyte can cause the performance

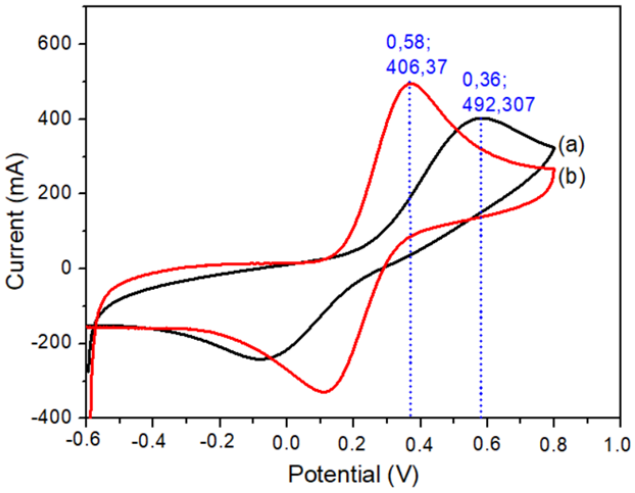

Figure 12. Cyclic voltammogram response of (a) GCE and (b) rGO modified GCE in 0.1 M NaCl

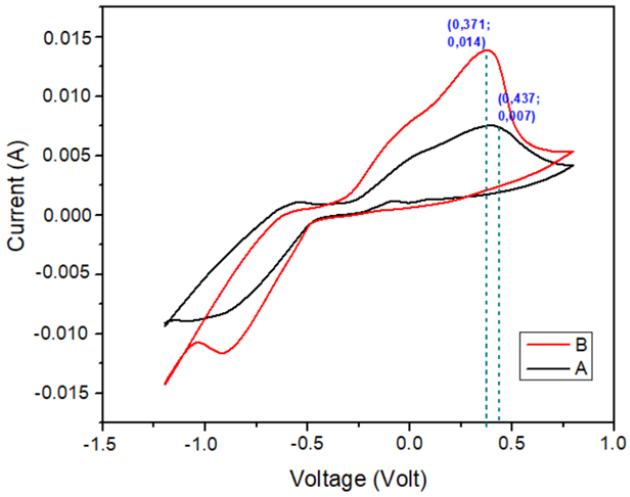

Figure 13. Cyclic voltammogram responses of (a) PbO_2 and (b) PbO_2/rGO in 0.1 M NaCl.

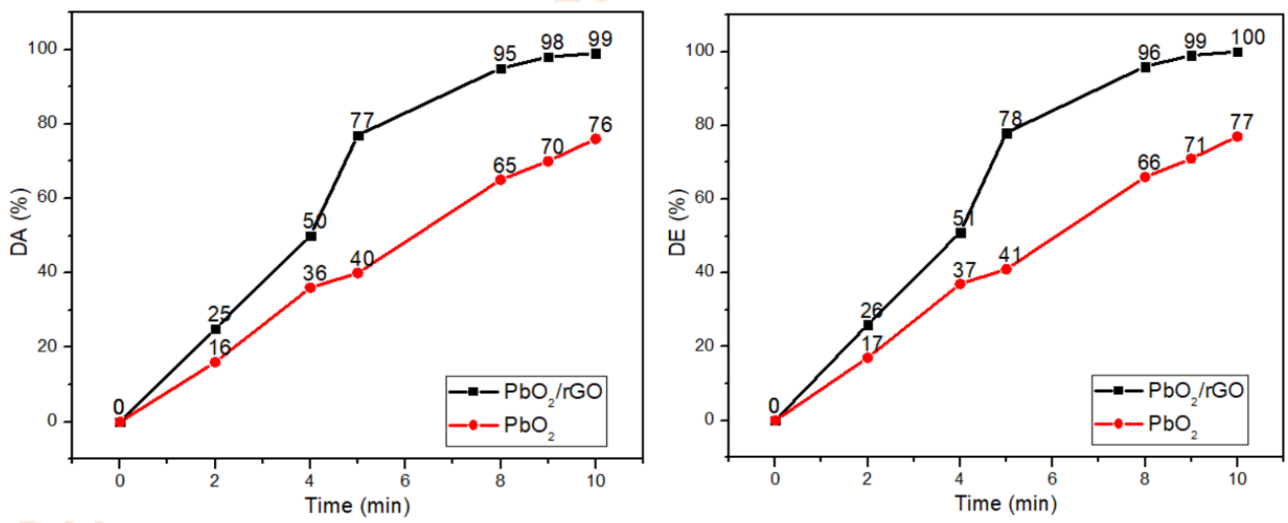

Figure 14. The process of removing the dye Safranine-O 20 ppm based on DA% and DE% using 0.1 M NaCl, current density 50 mA/cm2, and pH 7 with time variations on the electrodes

of the working electrode to decrease and be less stable, and NaCl can modulate the chemical species involved in the electrochemical reaction so that it can interfere with the degradation of specific dye compounds such as Safranine-O [72].

DA indicates a decrease in absorbance, and DE indicates degradation efficiency. Figures 14a and 14b show that DA is proportional to the DE. The longer the reaction time, the more dye compounds can be degraded, as evidenced by the increasing DA% and DE% data (Figures 14a and 14b). Similar studies have confirmed that the electrocatalysis time of dye degradation affects the extent of dye removal [33].

Figures 15a, 15b, and 15c show the results of the kinetics study of the data evaluated by applying the pseudo-first-order and pseudo-second-order kinetic equations. Based on the R^2 value, it can be concluded that the electrodegradation kinetics of Safranine-O using PbO_2 and PbO_2/rGO electrodes follow pseudo-first-order reaction kinetics. This is in accordance with previous studies showing that most dye electrodegradation follows pseudo-first-order reaction kinetics [97–99].

Figure 15d shows the decreasing absorbance process, indicating that Safranine-O is undergoing a degradation process. The decrease in the absorbance peak at 520 nm suggests that the auxochrome group has been degraded. Meanwhile, the decrease in absorbance in the 293 nm region indicates that the benzene ring structure or aromatic ring has been damaged [21,100]. The Safranine-O electrodegradation reaction, requiring the oxidizing agent •OH and Cl_2 and OCl^-, is shown in Equations (9–10) [96]. The main degradation mechanism of organic compounds, including Safranine-O ($C_{20}H_{19}N_4.Cl$) using PbO_2 anode, is the formation of ·OH, where ·OH is a strong oxidizing agent. The PbO_2 anode also allows reactions to occur:

$$PbO_2 + H_2O \rightleftharpoons PbO_2(\cdot OH) + H^+ + e^- \quad (9)$$

$$PbO_2(\cdot OH) + C_{20}H_{19}N_4.Cl \rightarrow PbO_2 + CO_2 + H_2O + \text{intermediate compounds} \quad (10)$$

The electrodegradation reaction of Safranin-O using a PbO_2 electrode with a NaCl electrolyte, apart from involving an oxidizing agent in the form of ·OH, also involves the oxidizing agents Cl_2 and ClO^- which are produced from the oxidation process of chloride ions in solution [96]. The reaction for the formation of Cl_2 and ClO^- is shown in Equations (11-12).

$$2Cl^- \rightarrow Cl_2 + 2e^- \quad (11)$$

$$Cl_2 + H_2O \rightarrow HOCl + H^+ + Cl^- \quad (12)$$

$$HClO \rightarrow H^+ + ClO^- \quad (13)$$

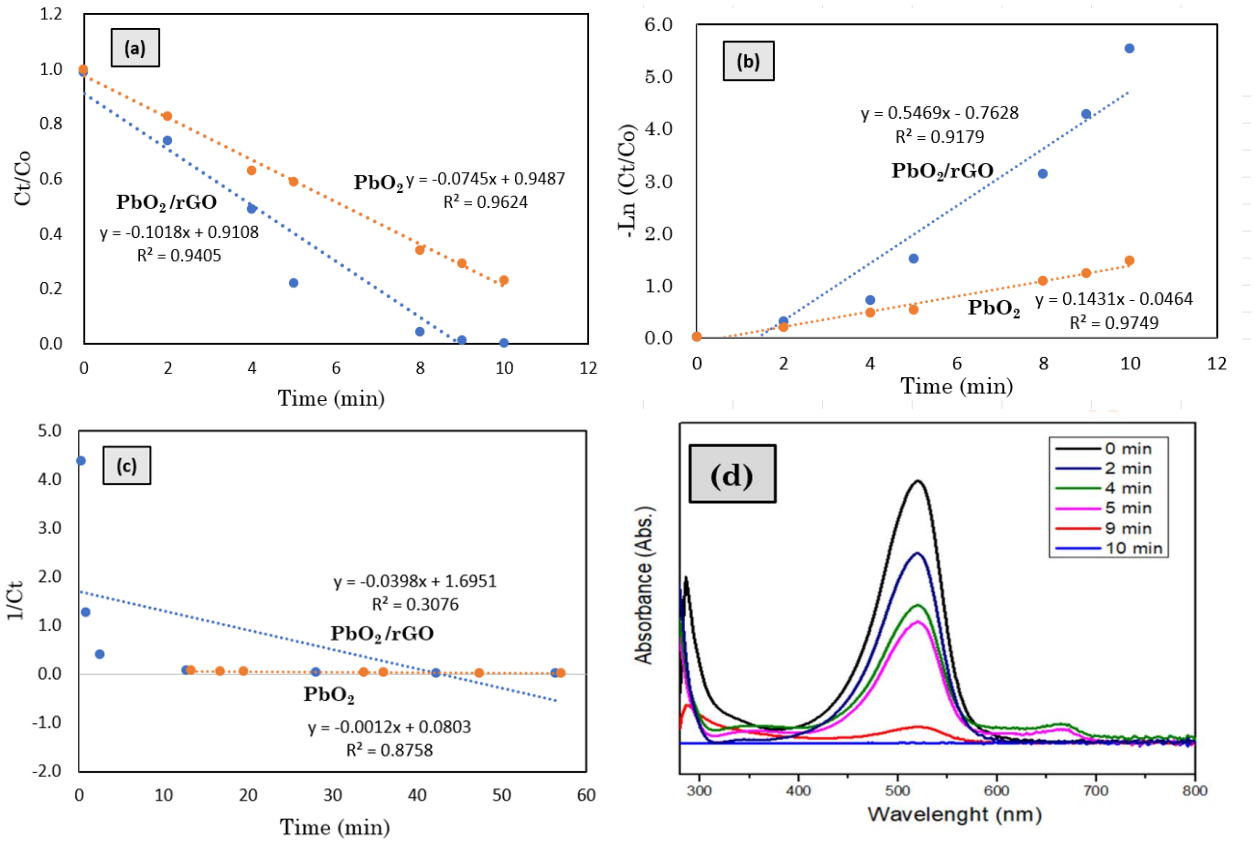

Figure 15. (a) Kinetics of Safranine-O removal by electrodegradation, (b). Pseudo-first-order kinetics plots, (c) Pseudo-second-order kinetics plots, (d). Uv-Vis Spectral change of Safranine-O spectra at varied Spectral change of Safranine-O spectra at varied treatment times by electrocatalytic degradation using PbO_2/rGO electrode, respectively.

When electrodegradation was carried out using PbO_2 and PbO_2/rGO anodes, it was seen that under the same operational conditions, the removal ability of Safranine-O on the PbO_2 anode was lower than the PbO_2/rGO electrode. This proves that adding rGO to the PbO_2 anode to become PbO_2/rGO can increase the electrocatalytic efficiency in Safranine-O degradation.

The great electrocatalytic degradation ability of the PbO_2/rGO anode is due to the electrocatalytic properties of the rGO layer, which can increase the conductivity of the anode and increase the formation of oxidants such as Cl_2 and ·OH. Using the NaCl electrolyte, the reaction in Equations 14–16 can occur in the electrocatalytic degradation of Safranine-O [21,101].

$$rG\text{-}OH \rightarrow rG\text{-}O^{\cdot} + H^+ + e^- \quad (14)$$
$$rG\text{-}O^{\cdot} + OH^- \rightarrow rG\text{-}O^- + {}^{\cdot}OH \quad (15)$$
$$rG\text{-}O^{\cdot} + Cl^- \rightarrow rG\text{-}O^- + Cl^{\cdot} \quad (16)$$
$$Cl^{\cdot} + Cl^- \rightarrow Cl_2 + e^- \quad (17)$$

The mechanism for the formation of hydroxyl radicals in electrodegradation is, firstly, the presence of a relatively high current density (50 mA/cm^2) that can oxidize rGO with hydroxyl groups (rG-OH) on the PbO_2/rGO anode to become rG-O· radicals. Secondly, rG-O· radicals undergo further reactions with OH^- ions from water ionization to form rG-O^- ions and hydroxyl radicals. Furthermore, the mechanism for the formation of chlorine (Cl_2) is that rG-O· radicals react with Cl^- ions resulting from ionization of the NaCl electrolyte to form Cl· radicals. Cl· radicals react further with Cl^- ions to form Cl_2 [68].

Based on the results of the electrocatalytic reactions that have been described, there are four types of oxidants in the PbO_2/rGO anode that play a role in the electrocatalysis of Safranine-O degradation, namely ·OH, Cl_2, and OCl^-. These oxidants react with Safranine-O to produce the final products CO_2 and H_2O.

$${}^{\cdot}OH + C_{20}H_{19}N_4.Cl \rightarrow OH^- + H_2O + \text{Intermediate compounds} \quad (18)$$

$$\text{Intermediate compounds} + {}^{\cdot}OH \rightarrow CO_2 + H_2O + OH^- \quad (19)$$

$$Cl_2 + C_{20}H_{19}N_4.Cl \rightarrow Cl^- + H_2O + \text{Intermediate compounds} \quad (20)$$

$$\text{Intermediate compounds} + Cl_2 \rightarrow CO_2 + H_2O + Cl^- \quad (21)$$

$$OCl^- + C_{20}H_{19}N_4.Cl \rightarrow Cl^- + H_2O + \text{Intermediate compounds} \quad (22)$$

$$\text{Intermediate compounds} + OCl^- \rightarrow Cl^- + CO_2 + H_2O \quad (23)$$

This study has also been related to reducing COD and BOD in Safranine-O and real waste containing Safranine-O waste after the electrodegradation process. The operational conditions of electrodegradation are using 0.1 M NaCl electrolyte, 0.5 A current, pH 7, and an initial concentration of Safranine-O. The real waste referred to in this study is waste from research and bacterial gram staining practical activities in the microbiology laboratory with initial COD and BOD values of 5562.5 mg/L and 1155 mg/L. The results can be seen in Table 2.

The electrochemical degradation of Safranine-O in this study (Table 2) showed that the PbO_2/rGO anode resulted in a greater increase in removal and decrease in BOD and COD values compared to electrochemical degradation using PbO_2 without rGO modification. This proves that rGO has good electrocatalytic ability when used as a PbO_2 anode modifier [30]. Compared with other research results, the Cationic Red X-GRL, Methyl Orange, and Methylene Blue dyes showed varying electrocatalytic degradation performance. These results indicate that the operational conditions of electrocatalytic degradation, such as current, pH, initial dye concentration, and electrolyte concentration and type, affect the performance of dye degradation [31,68].

In this study, lead (Pb) levels were measured in the electrolysis products using AAS to assess the stability of rGO on the electrode surface and the ability of rGO to prevent Pb dissolution on the PbO_2 anode. Pb dissolution data on the PbO_2 and PbO_2/rGO working electrodes after electrochemical degradation of Safranine-O are shown in Table 3. Measuring the Pb levels in the electrochemical degradation solution is important. This is because one of the weaknesses of the Pb electrode is the possibility of surface corrosion or the release of Pb^{2+} ions into the solution during the electrochemical degradation process at high current strengths, thus becoming new pollutants and causing new problems [36]. Table 3 shows that coating the PbO_2 anode with rGO can reduce the dissolution of Pb^{2+} ions in the solution during the electrochemical degradation process. The rGO coating has been shown to increase the stability of the PbO_2 anode, thereby reducing surface corrosion and Pb dissolution in the solution after the degradation process.

4. Conclusion

We applied the hydrothermal method on charcoal activated material to produce rGO. We used the EPD to synthesize the PbO_2/rGO electrode. The product has an element composition of C (78.60%) and O (21.40%). Application of PbO_2/rGO anode compared with PbO_2 anode on electrochemical degradation of Safranine-O 20 ppm and real waste showed better

Table 2. Removal of dye, reduction of BOD, and COD in electrochemical degradation

Dye	Operational Condition	Electrodes (Anode)	Removal of Dye (%)	Reduction of BOD (%)	Reduction of COD %	Ref.
Safranine-O	Current density 50 mA/cm², initial pH of solution 7, volume 100 mL, electrolyte NaCl 0.1 M, concentration 20 ppm	PbO_2	76 (10 min)	68 (10 min)	68 (10 min)	This study
Safranine-O	Current density 50 mA/cm², initial pH of solution 7, volume 100 mL, electrolyte NaCl 0.1 M, concentration 20 ppm	PbO_2/rGO	99 (10 min)	97 (10 min)	97 (10 min)	This study
Real waste	Current density 50 mA/cm², initial pH of solution 7, volume 100 mL, electrolyte NaCl 0.1 M	PbO_2/rGO	97 (10 min)	96 (10 min)	96 (10 min)	This study
Cationic Red X-GRL	Current density 3 mA/cm², initial pH of solution 5, Na_2SO_4 3 g/L, Volume 250 mL, concentration 300 mg/L	PbO_2/rGO/ ITO (ITO= Indium Tin Oxide)	88.4 (120 min)	-	35.7 (120 min)	[31]
Methyl Orange	Current density 50 mA/cm², initial pH of solution 9, NaCl 0.1 M, 20 ppm, Volume 100 mL, dye concentration 20 ppm	Pb/PbO_2/ rGO	98 (15 min)	-	-	[68]
Methylene Blue	Current density 10 mA/cm², initial pH of solution 5.4, Na_2SO_4 78.8 mg/L, concentration 60 mg/L	G/β-PbO_2 (G=graphite)	96.4 (50 min)	-	-	[66]

Table 3. Pb levels in solution after electrochemical degradation of Safranine-O

No	Electrodes	Time (minutes)	%DE	Pb level (ppm)
1	PbO_2	10	77	0.284
2	PbO_2/rGO	10	99	0.088

performance. It could remove dyes and reduce BOD and COD values by >95% within 10 minutes. Coating or modifying the PbO_2 anode with rGO was proven to increase the electrocatalytic ability of the electrode in solution during the electrochemical degradation process and reduce the dissolved Pb^{2+} ions.

Declaration of Competing Interest

The authors declare that they have no known competing financial interests or personal relationships that could have appeared to influence the work reported in this paper.

Acknowledgments

We thank the Ministry of Education, Culture, Research and Technology of the Republic of Indonesia for the Indonesian Education Scholarship (BPI) for providing Indonesian education scholarships (BPI) for doctoral study programs with number 00168/J5.2.3./BPI.06/9/2022.

CRediT Author Statement

Author Contributions: T. Aryani: Conceptualization, Investigation, Writing-Original draft, Software, Funding acquisition, Resources, Visualization, Data curation, Validation, Review & editing; R. Roto: Conceptualization, Writing, Methodology, Formal analysis, Resources, Data curation, Validation,

Review & editing, Supervision; M. Mudasir: Conceptualization, Formal analysis, Resources, Writing, Methodology, Validation, Data Curation, Review & editing, Supervision. All authors have read and agreed to the published version of the manuscript.

References

[1] El-Kemary, M., Abdel-Moneam, Y., Madkour, M., El-Mehasseb, I. (2011). Enhanced photocatalytic degradation of Safranin-O by heterogeneous nanoparticles for environmental applications. *Journal of Luminescence*, 131(4), 570–576. DOI: 10.1016/j.jlumin.2010.10.025.

[2] Pathania, D., Dhar, S., Sharma, A., Srivastava, A.K. (2021). Decolourization of noxious safranin-T from waste water using Mangifera indica as precursor. *Environmental Sustainability*, 4(2), 355–364. DOI: 10.1007/s42398-020-00130-0.

[3] Liu, B., Ren, B., Xia, Y., Yang, Y., Yao, Y. (2020). Electrochemical degradation of safranine T in aqueous solution by Ti/PbO2 electrodes. *Canadian Journal of Chemistry*, 98(1), 7–14. DOI: 10.1139/cjc-2019-0143.

[4] Eskikaya, O., Gun, M., Bouchareb, R., Bilici, Z., Dizge, N., Ramaraj, R., Balakrishnan, D. (2022). Photocatalytic activity of calcined chicken eggshells for Safranin and Reactive Red 180 decolorization. *Chemosphere*, 304, DOI: 10.1016/j.chemosphere.2022.135210.

[5] Granda-Ramírez, C.F., Hincapié-Mejía, G.M., Serna-Galvis, E.A., Torres-Palma, R.A. (2017). Degradation of Recalcitrant Safranin T Through an Electrochemical Process and Three Photochemical Advanced Oxidation Technologies. *Water, Air, and Soil Pollution*, 228(11), DOI: 10.1007/s11270-017-3611-2.

[6] Kiruthika, T., Poonkothai, M., Kalaiarasi, K., Ajarem, J.S., Allam, A.A., Khim, J.S., Sudhakar, C., Selvankumar, T., Alaguprathana, M. (2022). Decolorization of safranin using Fissidens species and its ecotoxicological assessments: An in vitro and in silico approach. *Environmental Research*, 211 DOI: 10.1016/j.envres.2022.113108.

[7] Li, W., Xie, Z., Xue, S., Ye, H., Liu, M., Shi, W., Liu, Y. (2021). Studies on the adsorption of dyes, Methylene blue, Safranin T, and Malachite green onto Polystyrene foam. *Separation and Purification Technology*, 276 DOI: 10.1016/j.seppur.2021.119435.

[8] Shariati, S., Faraji, M., Yamini, Y., Rajabi, A.A. (2011). Fe3O4 magnetic nanoparticles modified with sodium dodecyl sulfate for removal of safranin O dye from aqueous solutions. *Desalination*, 270(1–3), 160–165. DOI: 10.1016/j.desal.2010.11.040.

[9] Hamitouche, A., Benammar, S., Haffas, M., Boudjemaa, A., Bachari, K. (2016). Biosorption of methyl violet from aqueous solution using Algerian biomass. *Desalination and Water Treatment*, 57(34), 15862–15872. DOI: 10.1080/19443994.2015.1077476.

[10] Wang, X.Q., Wang, F.P., Zeng, X.H., Zhang, Q., Zhang, W., Le, J.Y., Yang, S.Z. (2015). Decolorization of methyl violet in simulated wastewater by dielectric barrier discharge plasma. *Japanese Journal of Applied Physics*, 54(5), DOI: 10.7567/JJAP.54.056201.

[11] Astuti, W., Sulistyaningsih, T., Maksiola, M. (2017). Equilibrium and kinetics of adsorption of methyl violet from aqueous solutions using modified Ceiba pentandra sawdust. *Asian Journal of Chemistry*, 29(1), 133–138. DOI: 10.14233/ajchem.2017.20158.

[12] Rahchamani, J., Mousavi, H.Z., Behzad, M. (2011). Adsorption of methyl violet from aqueous solution by polyacrylamide as an adsorbent: Isotherm and kinetic studies. *Desalination*, 267(2–3), 256–260. DOI: 10.1016/j.desal.2010.09.036.

[13] Beveridge, T.J. (2001). Use of the Gram stain in microbiology. *Biotechnic and Histochemistry*, 76(3), 111–118. DOI: 10.1080/bih.76.3.111.118.

[14] Becerra, S.C., Roy, D.C., Sanchez, C.J., Christy, R.J., Burmeister, D.M. (2016). An optimized staining technique for the detection of Gram positive and Gram negative bacteria within tissue. *BMC Research Notes*, 9(1), DOI: 10.1186/s13104-016-1902-0.

[15] Hayat, K., Gondal, M.A., Khaled, M.M., Yamani, Z.H., Ahmed, S. (2011). Laser induced photocatalytic degradation of hazardous dye (Safranin-O) using self synthesized nanocrystalline WO3. *Journal of Hazardous Materials*, 186(2–3), 1226–1233. DOI: 10.1016/j.jhazmat.2010.11.133.

[16] do Vale-Júnior, E., da Silva, D.R., Fajardo, A.S., Martínez-Huitle, C.A. (2018). Treatment of an azo dye effluent by peroxi-coagulation and its comparison to traditional electrochemical advanced processes. *Chemosphere*, 204, 548–555. DOI: 10.1016/j.chemosphere.2018.04.007.

[17] Setianingrum, N.P., Prasetya, A., Sarto, D. (2017). Pengurangan Zat Warna Remazol Red Rb Menggunakan Metode Elektrokoagulasi secara Batch. *Jurnal Rekayasa Proses*, 11(2), 78–85. DOI: 10.22146/jrekpros.26900.

[18] Bhatia, D., Sharma, N.R., Singh, J., Kanwar, R.S. (2017). Biological methods for textile dye removal from wastewater: A review. *Critical Reviews in Environmental Science and Technology*, 47(19), 1836–1876. DOI: 10.1080/10643389.2017.1393263.

[19] Bernal-Martínez, L.A., Barrera-Díaz, C., Solís-Morelos, C., Natividad, R. (2010). Synergy of electrochemical and ozonation processes in industrial wastewater treatment. *Chemical Engineering Journal*, 165(1), 71–77. DOI: 10.1016/j.cej.2010.08.062.

[20] Zhuo, Q., Luo, M., Guo, Q., Yu, G., Deng, S., Xu, Z., Yang, B., Liang, X. (2016). Electrochemical Oxidation of Environmentally Persistent Perfluorooctane Sulfonate by a Novel Lead Dioxide Anode. *Electrochimica Acta*, 213, 358–367. DOI: 10.1016/j.electacta.2016.07.005.

[21] Yusbarina, Y., Roto, R., Triyana, K. (2021). Hydroxyl functionalized graphene as a superior anode material for electrochemical oxidation of methylene blue. *Rasayan Journal of Chemistry*, 14(2), 1140–1147. DOI: 10.31788/RJC.2021.1426180.

[22] Sukarta, I.N., Kadek, N., Lusiani, S. (2008). Adsorpsi Zat Warna Azo Jenis Remazol Brilliant Blue Oleh Limbah Daun Ketapang (Terminalia Catappa L.). In: Prosiding Seminar Nasional Kimia UNY 2017 Sinergi Penelitian dan Pembelajaran untuk Mendukung Pengembangan Literasi Kimia pada Era Global Ruang Seminar FMIPA UNY, 14 Oktober 2017. pp. 311–316.

[23] Isarain-Chávez, E., Baró, M.D., Rossinyol, E., Morales-Ortiz, U., Sort, J., Brillas, E., Pellicer, E. (2017). Comparative electrochemical oxidation of methyl orange azo dye using Ti/Ir-Pb, Ti/Ir-Sn, Ti/Ru-Pb, Ti/Pt-Pd and Ti/RuO2 anodes. *Electrochimica Acta*, 244, 199–208. DOI: 10.1016/j.electacta.2017.05.101.

[24] Garcia-Segura, S., Ocon, J.D., Chong, M.N. (2018). Electrochemical oxidation remediation of real wastewater effluents — A review. *Process Safety and Environmental Protection*, 113, 48–67. DOI: 10.1016/j.psep.2017.09.014.

[25] Singh, S., Lien, S., Chandra, V., Devidas, A. (2016). Journal of Environmental Chemical Engineering Comparative study of electrochemical oxidation for dye degradation : Parametric optimization and mechanism identification. *Biochemical Pharmacology*, 4(3), 2911–2921. DOI: 10.1016/j.jece.2016.05.036.

[26] Shmychkova, O., Luk'Yanenko, T., Dmirtikova, L., Velichenko, A. (2019). Modified lead dioxide for organic wastewater treatment: Physicochemical properties and electrocatalytic activity. *Journal of the Serbian Chemical Society*, 84(2), 187–198. DOI: 10.2298/JSC180712091S.

[27] Radjenovic, J., Sedlak, D.L. (2015). Challenges and Opportunities for Electrochemical Processes as Next-Generation Technologies for the Treatment of Contaminated Water. *Environmental Science and Technology*, 49(19), 11292–11302. DOI: 10.1021/acs.est.5b02414.

[28] Liu, S., Wang, J., Zeng, J., Ou, J., Li, Z., Liu, X., Yang, S. (2010). "Green" electrochemical synthesis of Pt/graphene sheet nanocomposite film and its electrocatalytic property. *Journal of Power Sources*, 195(15), 4628–4633. DOI: 10.1016/j.jpowsour.2010.02.024.

[29] Clematis, D., Cerisola, G., Panizza, M. (2017). Electrochemical oxidation of a synthetic dye using a BDD anode with a solid polymer electrolyte. *Electrochemistry Communications*, 75, 21–24. DOI: 10.1016/j.elecom.2016.12.008.

[30] Soumya, M.S., Binitha, G., Praveen, P., Subramanian, K.R.V., Lee, Y.S., Shantikumar Nair, V., Sivakumar, N. (2015). Electrochemical performance of PbO2 and PbO2-CNT composite electrodes for energy storage devices. *Journal of Nanoscience and Nanotechnology*, 15(1), 703–708. DOI: 10.1166/jnn.2015.9172.

[31] Li, W., Yang, H., Liu, Q. (2017). Hydrothermal Synthesis of PbO2/RGO Nanocomposite for Electrocatalytic Degradation of Cationic Red X-GRL. *Journal of Nanomaterials*, 2017, DOI: 10.1155/2017/1798706.

[32] Nejati-Moghadam, L., Gholamrezaei, S., Salavati-Niasari, M., Esmaeili-Bafghi-Karimabad, A. (2017). Hydrothermal synthesis and characterization of lead oxide nanocrystal in presence of tetradentate Schiff-base and degradation investigation of organic pollutant in waste water. *Journal of Materials Science: Materials in Electronics*, 28(13), 9919–9926. DOI: 10.1007/s10854-017-6748-2.

[33] Awad, H.S., Galwa, N.A. (2005). Electrochemical degradation of Acid Blue and Basic Brown dyes on Pb/PbO2 electrode in the presence of different conductive electrolyte and effect of various operating factors. *Chemosphere*, 61(9), 1327–1335. DOI: 10.1016/j.chemosphere.2005.03.054.

[34] Gaber, M., Abu Ghalwa, N., Khedr, A.M., Salem, M.F. (2013). Electrochemical degradation of reactive yellow 160 dye in real wastewater using C/PbO2, Pb+Sn/PbO2+SnO, and Pb/PbO2 modified electrodes. *Journal of Chemistry*, 2013, 1–10. DOI: 10.1155/2013/691763.

[35] Widodo, D.S., Suyati, L., Gunawan, G., Haris, A. (2018). Decolorization of Artificial Waste Remazol Black B using Electrogenerated Reactive Spesies. *Jurnal Kimia Sains dan Aplikasi*, 21(1), 29–33. DOI: 10.14710/jksa.21.1.29-33.

[36] Bi, H., Yu, C., Gao, W., Cao, P. (2014). Physicochemical Characterization of Electrosynthesized PbO2 Coatings: The Effect of Pb2+ Concentration and Current Density. *Journal of The Electrochemical Society*, 161(6), D327–D332. DOI: 10.1149/2.032406jes.

[37] Irikura, K., Bocchi, N., Rocha-Filho, R.C., Biaggio, S.R., Iniesta, J., Montiel, V. (2016). Electrodegradation of the Acid Green 28 dye using Ti/ß-PbO2 and Ti-Pt/ß-PbO2 anodes. *Journal of Environmental Management*, 183, 306–313. DOI: 10.1016/j.jenvman.2016.08.061.

[38] Jiani, L., Zhicheng, X., Hao, X., Dan, Q., Zhengwei, L., Wei, Y., Yu, W. (2020). Pulsed electrochemical oxidation of acid Red G and crystal violet by PbO2 anode. *Journal of Environmental Chemical Engineering,* 8(3), 2–10. DOI: 10.1016/j.jece.2020.103773.

[39] Ghalwa, N.M.A., Zaggout, F.R. (2006). Electrodegradation of methylene blue dye in water and wastewater using lead oxide/titanium modified electrode. *Journal of Environmental Science and Health - Part A Toxic/Hazardous Substances and Environmental Engineering*, 41(10), 2271–2282. DOI: 10.1080/10934520600872888.

[40] Murthy, U.N., Rekha, H.B., Bhavya, J.G. (2011). Performance of Electrochemical Oxidation in Treating Textile Dye Wastewater by Stainless Steel Anode. *International Journal of Environmental Science and Development*, 2(6), 483–487. DOI: 10.7763/ijesd.2011.v2.174.

[41] Jin, X., Zhang, H., Wang, X., Zhou, M. (2012). An improved multi-anode contact glow discharge electrolysis reactor for dye discoloration. *Electrochimica Acta*, 59, 474–478. DOI: 10.1016/j.electacta.2011.11.001.

[42] Shmychkova, O., Luk'Yanenko, T., Dmirtikova, L., Velichenko, A. (2019). Modified lead dioxide for organic wastewater treatment: Physicochemical properties and electrocatalytic activity. *Journal of the Serbian Chemical Society*, 84(2), 187–198. DOI: 10.2298/jsc180712091S.

[43] Duan, X., Zhao, C., Liu, W., Zhao, X., Chang, L. (2017). Fabrication of a novel PbO2 electrode with a graphene nanosheet interlayer for electrochemical oxidation of 2-chlorophenol. *Electrochimica Acta*, 240, 424–436. DOI: 10.1016/j.electacta.2017.04.114.

[44] Shetti, N.P., Malode, S.J., Malladi, R.S., Nargund, S.L., Shukla, S.S., Aminabhavi, T.M. (2019). Electrochemical detection and degradation of textile dye Congo red at graphene oxide modified electrode. *Microchemical Journal*, 146, 387–392. DOI: 10.1016/j.microc.2019.01.033.

[45] Yan, L., Lin, M., Zeng, C., Chen, Z., Zhang, S., Zhao, X., Wu, A., Wang, Y., Dai, L., Qu, J., Guo, M., Liu, Y. (2012). Electroactive and biocompatible hydroxyl- functionalized graphene by ball milling. *Journal of Materials Chemistry*, 22(17), 8367–8371. DOI: 10.1039/c2jm30961k.

[46] Ahmad, F., Zahid, M., Jamil, H., Khan, M.A., Atiq, S., Bibi, M., Shahbaz, K., Adnan, M., Danish, M., Rasheed, F., Tahseen, H., Shabbir, M.J., Bilal, M., Samreen, A. (2023). Advances in graphene-based electrode materials for high-performance supercapacitors: A review. *Journal of Energy Storage*, 72, 108731, 1–17. DOI: 10.1016/j.est.2023.108731.

[47] Tene, T., Bellucci, S., Guevara, M., Romero, P., Guapi, A., Gahramanli, L., Straface, S., Caputi, L.S., Vacacela Gomez, C. (2024). Role of Graphene Oxide and Reduced Graphene Oxide in Electric Double-Layer Capacitors: A Systematic Review. *Batteries*, 10(7), 256. DOI: 10.3390/batteries10070256.

[48] Yang, J., Gunasekaran, S. (2013). Electrochemically reduced graphene oxide sheets for use in high performance supercapacitors. *Carbon*, 51(1), 36–44. DOI: 10.1016/j.carbon.2012.08.003.

[49] Lee, X.J., Hiew, B.Y.Z., Lai, K.C., Lee, L.Y., Gan, S., Thangalazhy-Gopakumar, S., Rigby, S. (2019). Review on graphene and its derivatives: Synthesis methods and potential industrial implementation. *Journal of the Taiwan Institute of Chemical Engineers*, 98, 163–180. DOI: 10.1016/j.jtice.2018.10.028.

[50] Bo, Z., Shuai, X., Mao, S., Yang, H., Qian, J., Chen, J., Yan, J., Cen, K. (2014). Green preparation of reduced graphene oxide for sensing and energy storage applications. *Scientific Reports*, 4(4864), 1–8. DOI: 10.1038/srep04684.

[51] Ahmad, S., Ahmad, A., Khan, S., Ahmad, S., Khan, I., Zada, S., Fu, P. (2019). Algal extracts based biogenic synthesis of reduced graphene oxides (rGO) with enhanced heavy metals adsorption capability. *Journal of Industrial and Engineering Chemistry*, 72, 117–124. DOI: 10.1016/j.jiec.2018.12.009.

[52] Qasim, S., Zafar, A., Saif, M.S., Ali, Z., Nazar, M., Waqas, M., Haq, A.U., Tariq, T., Hassan, S.G., Iqbal, F., Shu, X.G., Hasan, M. (2020). Green synthesis of iron oxide nanorods using Withania coagulans extract improved photocatalytic degradation and antimicrobial activity. *Journal of Photochemistry and Photobiology B: Biology*, 204(1), 1–11. DOI: 10.1016/j.jphotobiol.2020.111784.

[53] Alam, S.N., Sharma, N., Kumar, L. (2017). Synthesis of Graphene Oxide (GO) by Modified Hummers Method and Its Thermal Reduction to Obtain Reduced Graphene Oxide (rGO)*. *Graphene*, 06(01), 1–18. DOI: 10.4236/graphene.2017.61001.

[54] Shahriary, L., Athawale, A.A. (2014). Graphene Oxide Synthesized by using Modified Hummers Approach. *International Journal of Renewable Energy and Environmental Engineering*, 02(01), 1–8. DOI: 10.1016/j.jiec.2014.12.009.

[55] Fahrul, M., Hanifah, R., Jaafar, J., Aziz, M., Fauzi Ismail, A., Rahman, M.A., Hafiz, M., Othman, D. (2015). Synthesis of Graphene Oxide Nanosheets via Modified Hummers' Method and Its Physicochemical Properties. *Jurnal Teknologi*, 74, 2180–3722. DOI: 10.1039/c6ra02928k.

[56] Shams, S.S., Zhang, L.S., Hu, R., Zhang, R., Zhu, J. (2015). Synthesis of graphene from biomass: A green chemistry approach. *Materials Letters*, 161, 476–479. DOI: 10.1016/j.matlet.2015.09.022.

[57] Geetha Bai, R., Muthoosamy, K., Shipton, F.N., Pandikumar, A., Rameshkumar, P., Huang, N.M., Manickam, S. (2016). The biogenic synthesis of a reduced graphene oxide-silver (RGO-Ag) nanocomposite and its dual applications as an antibacterial agent and cancer biomarker sensor. *RSC Advances*, 6(43), 36576–36587. DOI: 10.1039/c6ra02928k.

[58] Fauzi Kurniawan, A. (2016). Sintesis Komposit Grafena Oksida Terduksi (rGO) Hasil Pembakaran Tempurung Kelapa Tua dengan Seng Oksida (ZnO) sebagai Superkapasitor. *Skripsi*. Surabaya: Program Studi Fisika; Institut Teknologi Sepuluh Nopember.

[59] Agus Putri, N., Arifin, Z., Supardi, I. (2023). Sintesis dan Karakterisasi Graphene Oxide (GO) dari Bahan Alam Tempurung Kelapa. *Jurnal Inovasi Fisika Indonesia (IFI)*, 12, 47–55. DOI: 10.26740/ifi.v12n2.p47-55.

[60] Sachdeva, H. (2020). Recent advances in the catalytic applications of GO/rGO for green organic synthesis. *Green Processing and Synthesis*, 9(1), 515–537. DOI: 10.1515/gps-2020-0055.

[61] Wang, M., Oh, J., Ghosh, T., Hong, S., Nam, G., Hwang, T., Nam, J. Do (2014). An interleaved porous laminate composed of reduced graphene oxide sheets and carbon black spacers by in situ electrophoretic deposition. *RSC Advances*, 4(7), 3284–3292. DOI: 10.1039/c3ra45979a.

[62] Yusbarina, Y., Roto, R., Triyana, K., Riau, S.K., Indonesia, R. (2021). Stainless Steel/Hydroxyl Functionalized Graphene Electrode for Electrochemical Oxidation of Methyl Orange, *Key Engineering Materials*, 884(1), 32-38. DOI: 10.31788/RJC.2021.1426180.

[63] Fatimah, I., Ramanda, G.D., Sagadevan, S., Suratno, Tamyiz, M., Doong, R. an (2024). One-pot synthesis of nickel nanoparticles-embedded biochar and insight on adsorption, catalytic oxidation and photocatalytic oxidation of dye. *Case Studies in Chemical and Environmental Engineering*, 10(0), 1–12. DOI: 10.1016/j.cscee.2024.100767.

[64] Nuraini, E., Fauziah, T., Lestari, F. (2019). Determination of BOD And COD Values of Inlet Waste Liquid Laboratory of Physical Testing ATK Polytechnic Yogyakarta. *Integrated Lab Journal*, 07(02) DOI: 10.5281/zenodo.3490306.

[65] Hait, M., Jaiswal, S. (2016). Removal of Water Pollutants from Industrial Waste Water of Korba Area by Bio-Adsorbents. *Journal of Scientific Letter*, 1(3), 223–229. DOI: 10.15294/ijcs.v3i1.2866.

[66] Samarghandi, M.R., Dargahi, A., Shabanloo, A., Nasab, H.Z., Vaziri, Y., Ansari, A. (2020). Electrochemical degradation of methylene blue dye using a graphite doped PbO2 anode: Optimization of operational parameters, degradation pathway and improving the biodegradability of textile wastewater. *Arabian Journal of Chemistry*, 13(8), 6847–6864. DOI: 10.1016/j.arabjc.2020.06.038.

[67] Shi, W., Fan, H., Ai, S., Zhu, L. (2015). Preparation of fluorescent graphene quantum dots from humic acid for bioimaging application. New Journal of Chemistry, 39(9), 7054–7059. DOI: 10.1039/c5nj00760g.

[68] Yusbarina (2021). Sintesis, Karakterisasi, dan Aplikasi Elektroda Pb/PbO2/rGO dan SS/G-OH pada elektrodegradasi Methylene Blue dan Methyl Orange. *PhD Disertasi*, 1–99. DOI: Departemen Kimia, Universitas Gadjah Mada.

[69] Kozyatnyk, I., Latham, K.G., Jansson, S. (2019). Valorization of Humic Acids by Hydrothermal Conversion into Carbonaceous Materials: Physical and Functional Properties. *ACS Sustainable Chemistry and Engineering*, 7(2), 2585–2592. DOI: 10.1021/acssuschemeng.8b05614.

[70] Soman, V., Vishwakarma, K., Poddar, M.K. (2023). Ultrasound assisted synthesis of polymer nanocomposites: a review. *Journal of Polymer Research*, 30(11), 3–15. DOI: 10.1007/s10965-023-03786-4.

[71] Setiadji, S., Nuryadin, B.W., Ramadhan, H., Sundari, C.D.D., Sudiarti, T., Supriadin, A., Ivansyah, A.L. (2018). Preparation of reduced Graphene Oxide (rGO) assisted by microwave irradiation and hydrothermal for reduction methods. *IOP Conference Series: Materials Science and Engineering*, 434(1) DOI: 10.1088/1757-899X/434/1/012079.

[72] Aprilia Nita (2019). Penggunaan Metode Ultrasonikasi dalam Proses Sintesis rGO dari Tempurung Kelapa. *Jurnal Inovasi Fisika Indonesi*a, 08(1), 8–10. DOI: 10.1039/c6ra02928k.

[73] Aryani, T., Aulia, I., Mu'awanah, U. (2023). Kajian Awal Sintesis Reduced Graphene Oxide (rGO) Metode Iradiasi Microwave dan Ultrasonikasi. *Jurnal Kolaboratif Sains*, 6(8), 1055–1060. DOI: 10.56338/jks.v6i8.3623.

[74] Htwe, Y.Z.N., Chow, W.S., Suda, Y., Thant, A.A., Mariatti, M. (2019). Effect of electrolytes and sonication times on the formation of graphene using an electrochemical exfoliation process. *Applied Surface Science*, 469, 951–961. DOI: 10.1016/j.apsusc.2018.11.029.

[75] Aguilar, J.C.S., Lawagon, C.P., Gallawan, J.M.M., Cabotaje, J.G. (2021). Hydroxyl-functionalized graphene from spent batteries as efficient adsorbent for amoxicillin. *Chemical Engineering Transactions*, 86, 331–336. DOI: 10.3303/CET2186056.

[76] Yan, J.A., Chou, M.Y. (2010). Oxidation functional groups on graphene: Structural and electronic properties. *Physical Review B - Condensed Matter and Materials Physics*, 82(12), 21–24. DOI: 10.1103/PhysRevB.82.125403.

[77] Ruidíaz-Martínez, M., Álvarez, M.A., López-Ramón, M.V., Cruz-Quesada, G., Rivera-Utrilla, J., Sánchez-Polo, M. (2020). Hydrothermal synthesis of RGO-TiO2 composites as high-performance UV photocatalysts for ethylparaben degradation. *Catalysts*, 10(5), 1–25. DOI: 10.3390/catal10050520.

[78] Intifadhah, S.H., Rohmawati, L., Setyarsih, W., Tukiran, T. (2018). The Effect of rGO Mass Composition on the Performance of Activated Carbon/rGO Supercapacitor Electrode Based on Coconut Shell (Cocos nucifera). In: Journal of Physics: Conference Series. *Institute of Physics Publishing*, DOI: 10.1088/1742-6596/1108/1/012045.

[79] Thema, F.T., Moloto, M.J., Dikio, E.D., Nyangiwe, N.N., Kotsedi, L., Maaza, M., Khenfouch, M. (2013). Synthesis and characterization of graphene thin films by chemical reduction of exfoliated and intercalated graphite oxide. *Journal of Chemistry*, 3, 1–7. DOI: 10.1155/2013/150536.

[80] Xiang, X., Zhu, Y., Gao, C., Du, H., Guo, C. (2022). Study on the structure of reduced graphene oxide prepared by different reduction methods. *Carbon Letters*, 32(2), 557–566. DOI: 10.1007/s42823-021-00287-6.

[81] Malard, L.M., Pimenta, M.A., Dresselhaus, G., Dresselhaus, M.S. (2009). Raman spectroscopy in graphene. *Physics Reports*, 473(5–6), 51–87. DOI: 10.1016/j.physrep.2009.02.003.

[82] Vázquez-Sánchez, P., Rodríguez-Escudero, M.A., Burgos, F.J., Llorente, I., Caballero-Calero, O., González, M.M., Fernández, R., García-Alonso, M.C. (2019). Synthesis of Cu/rGO composites by chemical and thermal reduction of graphene oxide. *Journal of Alloys and Compounds*, 800, 379–391. DOI: 10.1016/j.jallcom.2019.06.008.

[83] Mahmoud, A.E.D. (2020). Eco-friendly reduction of graphene oxide via agricultural byproducts or aquatic macrophytes. *Materials Chemistry and Physics*, 253, 1–9. DOI: 10.1016/j.matchemphys.2020.123336.

[84] Ali, G., Mehmood, A., Ha, H.Y., Kim, J., Chung, K.Y. (2017). Reduced graphene oxide as a stable and high-capacity cathode material for Na-ion batteries. *Scientific Reports*, 7(4), 1–8. DOI: 10.1038/srep40910.

[85] He, Z. (2018). Characterisation and Application of Lead Dioxide Electrodeposited from Methanesulfonate Electrolytes. *PhD Dissertation,* The University of Auckland.

[86] Amadelli, R., Velichenko, A.B. (2001). Lead dioxide electrodes for high potential anodic processes. *J. Serb. Chem. Soc.*, 66, 835–845. DOI: 10.2298/jsc0112835a.

[87] Smaili, F., Benchettara, A. (2019). Electrocatalytic Efficiency of PbO2 in Water Decontamination. *Russian Journal of Electrochemistry*, 55(10), 925–932. DOI: 10.1134/S1023193519100082.

[88] Behunová, D.M., Gallios, G., Girman, V., Kolev, H., Kaňuchová, M., Dolinská, S., Václavíková, M. (2021). Electrophoretic deposition of graphene oxide on stainless steel substrate. *Nanomaterials*, 11(7), 1–16. DOI: 10.3390/nano11071779.

[89] Chartarrayawade W, Moulton S. E., O. Too C, Wallace G.G (2013). Fabrication of graphene electrodes by electrophoretic deposition and their sinergistic effect with PEDOT and platinum. *Chiang Mai J. Sci.*, 40(4), 750–762. DOI: 10.1039/c6ra02928.

[90] Su, Y., Zhitomirsky, I. (2013). Electrophoretic deposition of graphene, carbon nanotubes and composite films using methyl violet dye as a dispersing agent. *Colloids and Surfaces A: Physicochemical and Engineering Aspects*, 436, 97–103. DOI: 10.1016/j.colsurfa.2013.06.024.

[91] Menéndez, R., Alvarez, P., Botas, C., Nacimiento, F., Alcántara, R., Tirado, J.L., Ortiz, G.F. (2014). Self-organized amorphous titania nanotubes with deposited graphene film like a new heterostructured electrode for lithium ion batteries. *Journal of Power Sources*, 248, 886–893. DOI: 10.1016/j.jpowsour.2013.10.019.

[92] Li, H., Zaviska, F., Liang, S., Li, J., He, L., Yang, H.Y. (2014). A high charge efficiency electrode by self-assembling sulphonated reduced graphene oxide onto carbon fibre: Towards enhanced capacitive deionization. *Journal of Materials Chemistry A*, 2(10), 3484–3491. DOI: 10.1039/c3ta14322h.

[93] Raza, M.A., Ali, A., Ghauri, F.A., Aslam, A., Yaqoob, K., Wasay, A., Raffi, M. (2017). Electrochemical behavior of graphene coatings deposited on copper metal by electrophoretic deposition and chemical vapor deposition. *Surface and Coatings Technology*, 332, 112–119. DOI: 10.1016/j.surfcoat.2017.06.083.

[94] Chen, J., Wu, J., Ge, H., Zhao, D., Liu, C., Hong, X. (2016). Reduced graphene oxide deposited carbon fiber reinforced polymer composites for electromagnetic interference shielding. *Composites Part A: Applied Science and Manufacturing*, 82, 141–150. DOI: 10.1016/j.compositesa.2015.12.008.

[95] Moura, D.C. De, Quiroz, M.A., Silva, D.R. Da, Salazar, R., Martínez-Huitle, C.A. (2016). Electrochemical degradation of Acid Blue 113 dye using TiO2-nanotubes decorated with PbO2 as anode. *Environmental Nanotechnology, Monitoring and Management*, 5, 13–20. DOI: 10.1016/j.enmm.2015.11.001.

[96] Mo, H., Chen, Y., Tang, Y., Li, T., Zhuang, S., Wang, L., Yang, X., Wan, P. (2019). Direct determination of chemical oxygen demand by anodic oxidative degradation of organics at a composite 3-D electrode. *Journal of Solid State Electrochemistry*, 23, 1571–1579. DOI: 10.1007/s10008-019-04250-4.

[97] Rajkumar, K., Muthukumar, M. (2017). Response surface optimization of electro-oxidation process for the treatment of C.I. Reactive Yellow 186 dye: reaction pathways. *Applied Water Science*, 7(2), 637–652. DOI: 10.1007/s13201-015-0276-0.

[98] Ghalwa, N.A., Abu-Shawish, H.M., Alharazeen, H., Tamous, H.M., Al Harazeen, H. (2013). Determination of Electrochemical Degradation of E102 Dye at Lead Dioxide-Doped Carbon Electrodes Using Some Potentiometric and Spectrophotometric Methods. *Chemistry Journal*, 03(1), 1–6. DOI: 10.1155/2013/691763.

[99] Değermenci, G.D. (2021). Removal of reactive azo dye using platinum-coated titanium electrodes with the electro-oxidation process. *Desalination and Water Treatment*, 218, 436–443. DOI: 10.5004/dwt.2021.26981.

[100] Yu, L., Xi, J., Li, M. De, Chan, H.T., Su, T., Phillips, D.L., Chan, W.K. (2012). The degradation mechanism of methyl orange under photo-catalysis of TiO2. *Physical Chemistry Chemical Physics*, 14(10), 3589–3595. DOI: 10.1039/c2cp23226j.

[101] Mukimin, A., Vistanty, H., Zen, N. (2015). Oxidation of textile wastewater using cylinder Ti/ß-PbO2 electrode in electrocatalytic tube reactor. *Chemical Engineering Journal*, 259, 430–437. DOI: 10.1016/j.cej.2014.08.020.